Mathematical Models in Biology

Hermann Riecke

Engineering Sciences and Applied Mathematics

Northwestern University

h-riecke@northwestern.edu

June 5, 2018

Contents

[1] (Keller and Segel, 1971a)
[2] (Keller and Segel, 1971b)
[3] worthwhile video by H. Berg: https://www.youtube.com/watch?v=ioA1yuIA-t8
[4] (Tu and Rappel, 2018)

References

Adler J. (1966a). Chemotaxis in bacteria. Science *153*, 708–&.

Adler J. (1966b). Effect of amino acids and oxygen on chemotaxis in escherichia coli. Journal of Bacteriology *92*, 121–&.

Adler J., and Dahl M.M. (1967). A method for measuring motility of bacteria and for comparing random and non-random motility. Journal of General Microbiology *46*, 161–&.

Alon U. (2007). An Introduction to Systems Biology (Chapman & Hall).

Artemenko Y., Lampert T.J., and Devreotes P.N. (2014). Moving towards a paradigm: common mechanisms of chemotactic signaling in dictyostelium and mammalian leukocytes. Cellular and molecular life sciences : CMLS *71*, 3711–3747.

Barkai N., and Leibler S. (1997). Robustness in simple biochemical networks. Nature *387*, 913–917.

Berg H.C., and Brown D.A. (1972). Chemotaxis in escherichia-coli analyzed by 3-dimensional tracking. Nature *239*, 500–&.

Berg H.C., and Purcell E.M. (1977). Physics of chemoreception. Biophysical journal *20*, 193–219.

Brown D.A., and Berg H.C. (1974). Temporal stimulation of chemotaxis in eschericia coli. PNAS .

Browne E.N. (1909). The production of new hydranths in hydra by the insertion of small grafts. Journal of Experimental Zoology *7*, 1–U13.

Crick F. (1970). Diffusion in embryogenesis. Nature *225*, 420–422.

Dahlquis F., Lovely P., and Koshland D.E. (1972). Quantitative analysis of bacterial migration in chemotaxis. Nature-new Biology *236*, 120–&.

Driever W., and Nusslein-Volhard C. (1988). A gradient of bicoid protein in drosophila embryos. Cell *54*, 83–93.

Driver W., Siegel V., and Nusslein-Volhard C. (1990). Autonomous determination of anterior structures in the early drosophila embryo by the bicoid morphogen. Development *109*, 811–820.

Eldar A., Rosin D., Shilo B.Z., and Barkai N. (2003). Self-enhanced ligand degradation underlies robustness of morphogen gradients. Developmental Cell *5*, 635–646.

Goldstein R. (1996). Traveling-wave chemotaxis. Phys. Rev. Lett. *77*, 775.

Gregor T., Bialek W., de Ruyter van Steveninck R.R., Tank D.W., and Wieschaus E.F. (2005). Diffusion and scaling during early embryonic pattern formation. Proceedings of the National Academy of Sciences of the United States of America *102*, 18403–18407.

Grimm O., Coppey M., and Wieschaus E. (2010). Modelling the bicoid gradient. Development *137*, 2253–2264.

Harland R. (2008). Induction into the hall of fame: tracing the lineage of spemann's organizer. Development (Cambridge, England) *135*, 3321–3323.

Houchmandzadeh B., Wieschaus E., and Leibler S. (2002). Establishment of developmental precision and proportions in the early drosophila embryo. Nature *415*, 798–802.

Houchmandzadeh B., Wieschaus E., and Leibler S. (2005). Precise domain specification in the developing drosophila embryo. Physical review. E, Statistical, nonlinear, and soft matter physics *72*, 061920.

Jaeger J. (2009). Modelling the drosophila embryo. Molecular Biosystems *5*, 1549–1568.

Keller E.F., and Segel L.A. (1971a). Model for chemotaxis. Journal of Theoretical Biology *30*, 225–&.

Keller E.F., and Segel L.A. (1971b). Traveling bands of chemotactic bacteria - theoretical analysis. Journal of Theoretical Biology *30*, 235–&.

Kessler D., and Levine H. (1993). Pattern-formation in Dictyostelium via the dynamics of cooperative biological entities. Phys. Rev. E *48*, 4801.

Lapidus I.R., and Schiller R. (1976). Model for the chemotactic response of a bacterial population. Biophysical journal *16*, 779–789.

Larsen S.H., Reader R.W., Kort E.N., Tso W.W., and Adler J. (1974). Change in direction of flagellar rotation is basis of chemotactic response in escherichia-coli. Nature *249*, 74–77.

Little S.C., Tkacik G., Kneeland T.B., Wieschaus E.F., and Gregor T. (2011). The formation of the bicoid morphogen gradient requires protein movement from anteriorly localized mrna. PLoS biology *9*, e1000596.

Macnab R.M., and Koshland D.E. (1972). The gradient-sensing mechanism in bacterial chemotaxis. Proceedings of the National Academy of Sciences of the United States of America *69*, 2509–2512.

McHale P., Rappel W.J., and Levine H. (2006). Embryonic pattern scaling achieved by oppositely directed morphogen gradients. Phys. Biol. *3*, 107–120.

Mears P.J., Koirala S., Rao C.V., Golding I., and Chemla Y.R. (2014). Escherichia coli swimming is robust against variations in flagellar number. eLife *3*, e01916. Original DateCompleted: 20140212.

Meinhardt H. (1993). A model for pattern formation of hypostome, tentacles, and foot in hydra: how to form structures close to each other, how to form them at a distance. Developmental biology *157*, 321–333.

Meinhardt H. (2012). Turing's theory of morphogenesis of 1952 and the subsequent discovery of the crucial role of local self-enhancement and long-range inhibition. Interface focus *2*, 407–416.

Mello B.A., Shaw L., and Tu Y.H. (2004). Effects of receptor interaction in bacterial chemotaxis. Biophysical Journal *87*, 1578–1595.

Mesibov R., Ordal G.W., and Adler J. (1973). The range of attractant concentrations for bacterial chemotaxis and the threshold and size of response over this range. weber law and related phenomena. The Journal of general physiology *62*, 203–223.

Nakajima A., Ishihara S., Imoto D., and Sawai S. (2014). Rectified directional sensing in long-range cell migration. Nature communications *5*, 5367.

Noorbakhsh J., Schwab D.J., Sgro A.E., Gregor T., and Mehta P. (2015). Modeling oscillations and spiral waves in dictyostelium populations. Physical review. E, Statistical, nonlinear, and soft matter physics *91*, 062711.

Othmer H.G., Xin X.R., and Xue C. (2013). Excitation and adaptation in bacteria-a model signal transduction system that controls taxis and spatial pattern formation. International Journal of Molecular Sciences *14*, 9205–9248.

Purves W., an d G.H. Orians D.S., and Heller H. (1998). Life: The Science of Biology.

Sgro A.E., Schwab D.J., Noorbakhsh J., Mestler T., Mehta P., and Gregor T. (2015). From intracellular signaling to population oscillations: bridging size- and time-scales in collective behavior. Molecular systems biology *11*, 779.

Sourjik V. (2004). Receptor clustering and signal processing in e coli chemotaxis. Trends in Microbiology *12*, 569–576.

Sourjik V., and Berg H.C. (2002). Receptor sensitivity in bacterial chemotaxis. Proceedings of the National Academy of Sciences of the United States of America *99*, 123–127.

Spemann H., and Mangold H. (1924). The induction of embryonic predispositions by implantation of organizers foreign to the species. Archiv Fur Mikroskopische Anatomie Und Entwicklungsmechanik *100*, 599–638.

Tindall M.J., Maini P.K., Porter S.L., and Armitage J.P. (2008). Overview of mathematical approaches used to model bacterial chemotaxis ii: Bacterial populations. Bulletin of Mathematical Biology *70*, 1570–1607.

Tu Y.H., and Rappel A.J. (2018). Adaptation in living systems. Annual Review of Condensed Matter Physics, Vol 9 *9*, 183–205.

Turing A.M. (1952). The chemical basis of morphogenesis. Phil. Trans. Roy. Soc. London B *237*, 5.

Wolpert L. (1969). Positional information and spatial pattern of cellular differentiation. Journal of Theoretical Biology *25*, 1–&.

1 Chemotaxis

Chemotaxis has already been observed in the late 1800's by Engelmann, Pfeffer, and others.

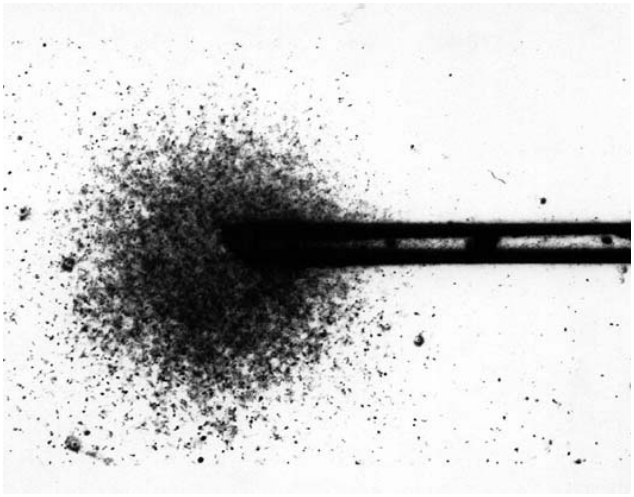

Figure 1: Aggregation of chemotactic bacteria in regions of high concentration of an attractant (Pfeffer 1888 in (Tindall et al., 2008))

Chemotaxis plays an important role in many aspects of the life of organisms (Artemenko et al., 2014)

- Cell migration plays an important role in development; it is partially guided by chemotaxis
- Trafficking immune cells to sites of inflammation; incorrect chemotaxis of leukocytes contributes to chronic inflammation diseases like arthritis
- Cancer metastasis: tumor cells searching for blood vessels

1.1 Chemotaxis of Bacteria

Bacteria are much simpler than eukaryots (cells with nucleus). But understanding their chemotaxis may give insight also into the chemosensation in higher animals.

Experiments by Adler

- bacteria (escherichia coli) placed at one end of tube filled with food (glucose, galactose, amino acids)
- migrate into the tube
- two bands are formed
- the first band uses up all the oxygen and 20% of the galactose

- the second band uses up the remaining galactose in some anaerobic process
- in two dimensions rings form and the bands stop when they collide

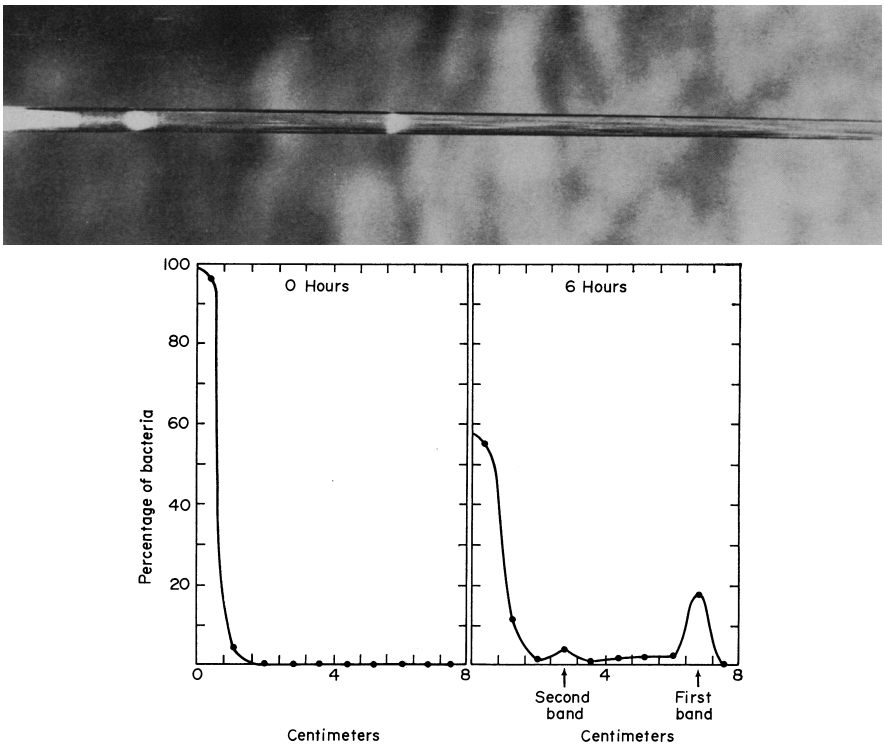

Figure 2: a) Two traveling bands of migrating *E. coli* bacteria emerge when they are placed in a tube with a chemoattractant at one end. b) Quantification of the bacteria concentration. (Adler, 1966a)

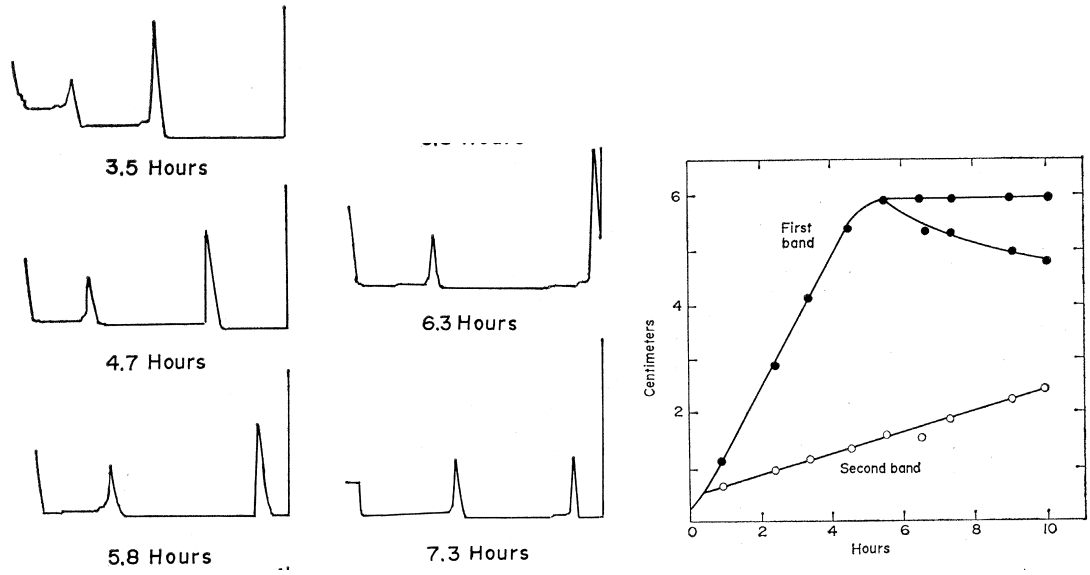

Figure 3: Motion of the two bands and quantification of their position as a function of time. The second band propagates more slowly (Adler, 1966a). Note that the velocity of the fronts is quite constant in time until they hit the end of the capillary.

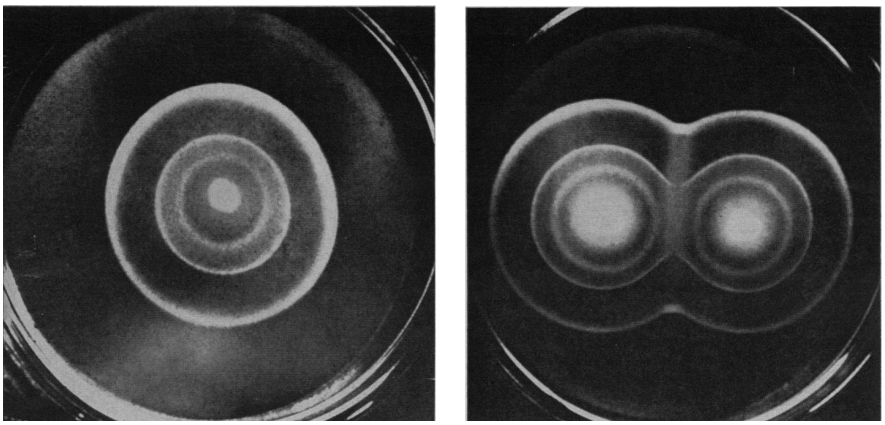

Figure 4: *E. coli* bacteria deposited in the center of an agar plate swarm out forming rings, which annihilate when they collide (Adler, 1966a).

What are individual bacteria doing in these bands and in chemical gradients?

- the 'avoiding reaction' was already observed by the end of the 19th century (Engelmann, Pfeffer, Rothert, Jennings, cf. Fig.1)
  - when a bacterium enters a low concentration region it stops suddenly, 'looks disoriented', and continues swimming in some new direction: the motion of the bacterium consists of 'runs' and 'tumbles'
  - in some species that can swim forward and backward the bacteria reverse direction if they enter a low-concentration region

- by avoiding the low concentration regions the bacteria eventually accumulate in the regions with higher concentration
  - there are also species that avoid high concentrations and accumulate at low concentrations
  - extremely high concentrations are often avoided as well.

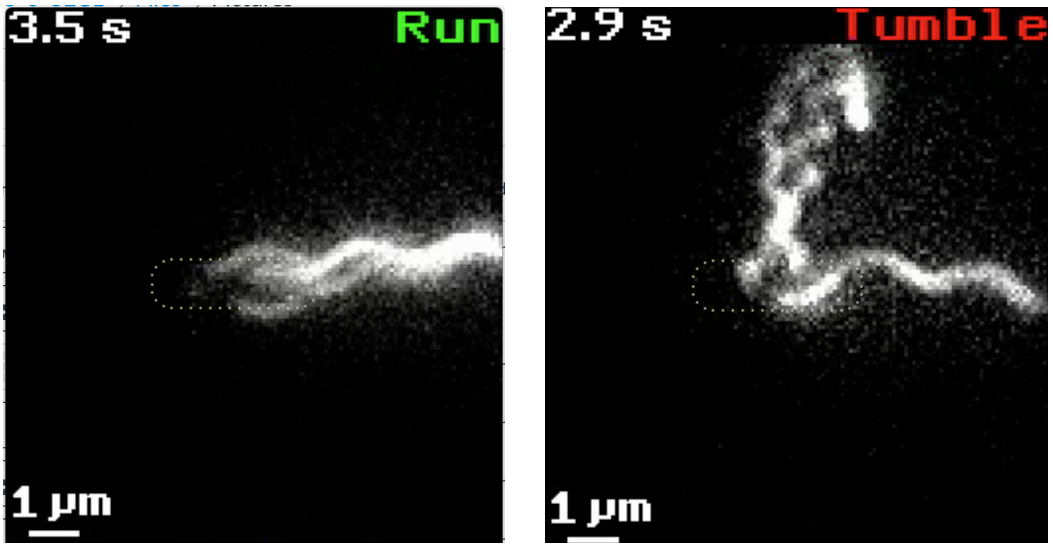

Figure 5: *E. coli* swimming. a) During swimming all three flagella are interwined when they are rotating counter-clockwise (CCW). b) When the flagella rotate clockwise (CW), they become disordered and the bacterium tumbles. Dashed line indicates body of the bacterium, which was not marked. For video see Canvas or the online version of the paper (Mears et al., 2014)

Note:

- Since in biology many aspects (genetics, metabolism) are conserved across very different species and chemosensation is a very old sense, Adler proposes that the nervous system and the behavior of higher organisms may have evolved from chemical reactions operating in the 'most primitive living things' (Adler, 1966a).

Modeling questions:

- What long-time dynamics results from run-and-tumble? How to describe the dynamics of a population of such bacteria?
- What are limits for the sensing capabilities of very small organisms like bacteria?
- How can a bacterium sense a chemical gradient
  - the observation of run-and-tumble suggests that it may not need to sense the gradient itself; sensing the concentration as such may be enough, if its motion takes it to locations with different concentrations, which it then compares.

- but: does it tumble all the time when the overall concentration is low and run all the time when the concentration is high? How does it then effectively compare two different high concentrations or two low concentrations?

1.2 Modeling Chemotactic Motion [5]

Based on the run-and-tumble observation, Keller and Segel developed a continuum model for the concentration of a population of bacteria.

Bacteria move by propelling themselves forward with flagella; depending on species, the flagella pull or push the bacterium.

Assume

- during a run the bacterium moves a fixed distance
- between runs the bacteria tumble, i.e. the new direction of motion after the tumbling is not correlated with the direction before the tumbling
- the average frequency of runs depends on the concentration at the leading edge of the bacterium (could instead also use the trailing edge), i.e. the receptor sensing the chemical is at the leading (or trailing) end
- the concentration does not change a lot over distances corresponding to a single run.

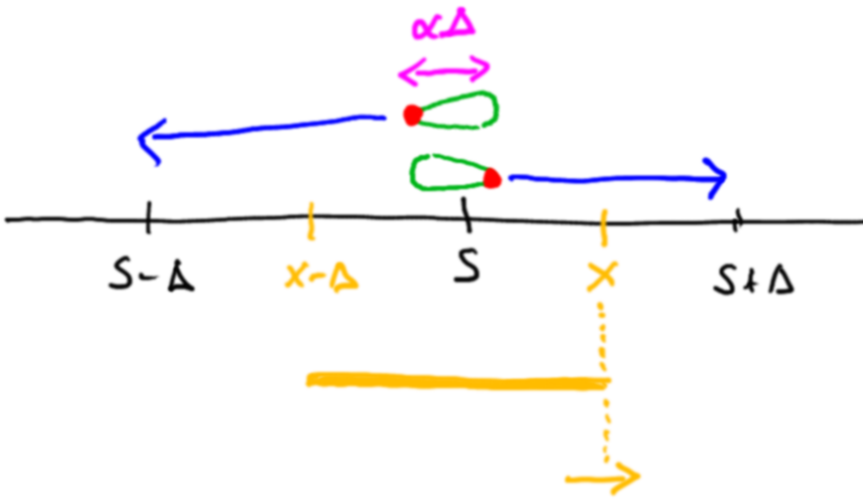

Figure 6: Bacteria of size $\alpha\Delta$ with sensors at their leading edge running a distance Δ.

For simplicity, consider only motion in 1 dimension

- during each run a bacterium moves a distance $\pm\Delta$
- because of the tumbles the probability for motion to the right is equal to that to the left

[5] (Keller and Segel, 1971a)

- the bacterium has an effective size of $\alpha\Delta$, i.e. the sensors of right- and left-moving bacteria at a given location are a distance $\alpha\Delta$ apart.

We want an equation for the evolution of the density of bacteria $b(x)$.

Consider the flux $J(x)$ through the location x during a short time interval Δt. This time interval could be the typical time between tumbles and in each time step half of the population would be oriented to the left and half to the right. The flux is considered positive if the motion is to the right.

- if the average frequency of a run is f then the probability of a run for a given bacterium during the time interval Δt is given by $f\Delta t$. The fraction of the population doing a run is then $f\Delta t$.
- all bacteria at a location s within $[x-\Delta, x]$ that move to the right will pass the location x during this step; their frequency depends on the concentration at $s + \frac{1}{2}\alpha\Delta$, where s is their location within that interal.
- all bacteria at a location s within $[x, x+\Delta]$ that move to the left will pass the location x during this step; their frequency depends on the concentration at $s - \frac{1}{2}\alpha\Delta$.

The total number of bacteria passing through the point x during the time interval Δt is then

$$J(x)\Delta t = \int_{x-\Delta}^{x} f\left(c(s+\frac{1}{2}\alpha\Delta)\right)\Delta t\, b(s)\, ds - \int_{x}^{x+\Delta} f\left(c(s-\frac{1}{2}\alpha\Delta)\right)\Delta t\, b(s)\, ds$$

Since the run size Δ is small compared to the lengths over which the concentrations changes, we can expand in Δ

$$\int_{x-\Delta}^{x} f\left(c(s+\frac{1}{2}\alpha\Delta)\right)\, b(s)\, ds = \int_{x-\Delta}^{x} \left\{ f\left(c(s)\right) + \underbrace{f'\left(c(s)\right)c'(s)\frac{1}{2}\alpha\Delta}_{f'(c(x))c'(x)\frac{1}{2}\alpha\Delta+\mathcal{O}(\Delta^2)} + \mathcal{O}(\Delta^2) \right\} b(s)\, ds$$

where $f'(c) = \frac{df(c)}{dc}$ and $c'(x) = \frac{dc(x)}{dx}$. Expand also

$$\begin{aligned} f\left(c(s)\right) &= f\left(c(x)\right) + (s-x)f'(c(x))c'(x) + \mathcal{O}\left((s-x)^2\right) \\ b(s) &= b(x) + (s-x)b'(x) + \mathcal{O}\left((s-x)^2\right) \end{aligned}$$

Then

$$\begin{aligned} \int_{x-\Delta}^{x} f\left(c(s)\right) b(s) ds &= \int_{x-\Delta}^{x} f\left(c(x)\right) b(x) + (s-x)\left[f'(c(x))c'(x)b(x) + f(c(x))b'(x)\right] + \mathcal{O}\left((s-x)^2\right)\, ds \\ &= f\left(c(x)\right) b(x)\,\Delta + \left[f'(c(x))c'(x)b(x) + f(c(x))b'(x)\right] \underbrace{\frac{1}{2}\left(s-x\right)^2\Big|_{x-\Delta}^{x}}_{-\frac{1}{2}\Delta^2} + \mathcal{O}\left(\Delta^3\right) \end{aligned}$$

Analogously

$$\int_x^{x+\Delta} f\left(c(s-\frac{1}{2}\alpha\Delta)\right)\, b(s)\, ds = \int_x^{x+\Delta} \left\{ f\left(c(s)\right) - \underbrace{f'\left(c(s)\right) c'(s) \frac{1}{2}\alpha\Delta}_{f'(c(x))c'(x)\frac{1}{2}\alpha\Delta+\mathcal{O}(\Delta^2)} + \mathcal{O}(\Delta^2) \right\} b(s)\, ds$$

with

$$\begin{aligned}
\int_x^{x+\Delta} f\left(c(s)\right) b(s) ds &= \int_x^{x+\Delta} f\left(c(x)\right) b(x) + (s-x)\left(f'(c(x))c'(x)b(x) + f(c(x))b'(x)\right) + \mathcal{O}\left((s-x)^2\right)\, ds \\
&= f\left(c(x)\right) b(x)\, \Delta + \left[f'(c(x))c'(x)b(x) + f(c(x))b'(x)\right] \underbrace{\frac{1}{2}\left(s-x\right)^2\Big|_x^{x+\Delta}}_{\frac{1}{2}\Delta^2} + \mathcal{O}\left(\Delta^3\right)
\end{aligned}$$

Combined

$$\begin{aligned}
J(x) &= -\left[f'\left(c(x)\right) c'(x) b(x) + f(c(x))b'(x)\right]\, \Delta^2 + f'\left(c(x)\right) c'(x)\alpha\Delta^2 b(x) + \mathcal{O}\left(\Delta^3\right) \\
&= -\left\{f'\left(c(x)\right) c'(x) b(x)\left(1-\alpha\right) + f(c(x))b'(x)\right\}\Delta^2 \\
&= -\mu\frac{db}{dx} + \chi b\frac{dc}{dx}
\end{aligned}$$

with

$$\begin{aligned}
\mu(c) &= f(c)\Delta^2 \\
\chi(c) &= \left(\alpha-1\right) f'(c)\Delta^2 = \left(\alpha-1\right)\mu'(c)
\end{aligned}$$

To get an evolution equation for the density we use conservation of bacteria in a little 'volume' $[x-dx, x+dx]$ around x

$$2dx\frac{\partial b}{\partial t} = J(x-dx) - J(x+dx) = -2\frac{\partial J}{\partial x}dx + \mathcal{O}(dx^2)$$

Thus

$$\frac{\partial b}{\partial t} = -\frac{\partial}{\partial x}\left(-\mu\frac{\partial b}{\partial x} + \chi b\frac{\partial c}{\partial x}\right) \tag{1}$$

Notes:

- μ is called the motility coefficient. It is always positive.
- With $f(c)$ being the average frequency of steps, $\Delta t \equiv \frac{1}{f(c)}$ is the average time betwen steps

  $$\mu = \frac{\Delta^2}{\Delta t}$$

  Thus, if f is independent of concentration we get

  $$\frac{\partial b}{\partial t} = \mu\frac{\partial^2 b}{\partial x^2}$$

i.e., the bacteria move in a diffusive manner: they perform a random walk (Adler and Dahl, 1967).
Consider random steps with equal probability $\pm\Delta$

$$\langle x\rangle = \left\langle \sum_{i=1}^{N} \Delta_i \right\rangle = \sum_{i=1}^{N} \langle \Delta_i\rangle = 0$$

$$\langle x^2\rangle \;=\; \left\langle \left(\sum_{i=1}^{N}\Delta_i\right)\left(\sum_{j=1}^{N}\Delta_j\right)\right\rangle = \left\langle \sum_{i=1}^{N}\sum_{j=1}^{N}\Delta_i\Delta_j\right\rangle \underbrace{=}_{\text{uncorrelated}} \sum_{i=1}^{N}\langle\Delta_i^2\rangle = N\Delta^2$$

If each step takes a time Δt, the motility (diffusion) coefficient μ is the increase in the variance of the position per time step.

- χ is called the chemotactic coefficient.

The chemotactic coefficient can have either sign

$\chi \gtrless 0$ bacteria move towards higher/lower values of the concentration

It depends on $f'(c)$ and on α.

- $\alpha = 0$: the bacterium is extremely small $\chi = -\mu' = -f'\Delta^2$
  $\chi > 0$ if the average frequency of steps f decreases with concentration, i.e. the bacteria are less likely to leave the higher concentration than the lower concentration.
  This is the run-and-tumble situation, in which the bacteria do not measure instantaneous concentration differences.

- $\alpha < 1$: the sign of χ is opposite to that of f' (as in the case of $\alpha = 0$)
  consider the bacteria at the mean position in the left interval

$$f\left(c\left(x - \frac{1}{2}\Delta + \frac{1}{2}\alpha\Delta\right)\right) = f\left(c\left(x + \frac{1}{2}(\alpha - 1)\Delta\right)\right)$$

  For $\alpha < 1$ the frequency for motion to the right depends on the concentration to the left of x and the frequency for motion to the left on the concentration to the right of x
  $\rightarrow$ for the bacteria to move predominantly to the right if the concentration is higher there, one needs $f'(c) < 0$ to have them be more likely to do a run on the left than on the right.

- $\alpha > 1$: the runs are shorter than the size of the bacteria: to get $\chi > 0$ one needs now $f'(c) > 0$.

Simple Explicit Model

Bacteria are small and their sensors are even smaller: they can only measure the concentration in a very small volume, which contains only few molecules of the sensed chemical $\Rightarrow$ the measured concentrations ξ fluctuate strongly. But the bacterium has to base its motion on these fluctuating values. Consider a simple stochastic model.

Assume that $f(\xi)$ has only two values

$$f(\xi) = \begin{cases} k & \text{for } \xi > Q \\ k\left(1-\bar{k}\right) & \text{for } \xi \le Q \end{cases}$$

with $\bar{k} \le 1$.

For $\bar{k} > 0$ the frequency increases with increasing concentration $\Rightarrow$ expect $\chi > 0$ only for $\alpha > 1$.

For $c = \langle \xi \rangle$ the average number of steps taken is then

$$\bar{f}(c) = k\left\{1 \cdot P(\xi > Q) + (1-\bar{k})P(\xi \le Q)\right\} = k\left\{1 - \bar{k}\,\mathcal{P}(\xi \le Q)\right\}.$$

With the probability distribution of ξ given by $F(\xi; c)$ we have then

$$\mu = \Delta^2 \bar{f}(c) = \Delta^2 k \left\{1 - \bar{k}\int_0^Q F(\xi; c)\, d\xi\right\}$$

Limiting cases can be recognized already for any reasonable distribution $F(\xi; c)$

$c \to 0$: almost always $\xi < Q$

$$\mu \to \Delta^2 k\left(1-\bar{k}\right)$$

$c \to \infty$: almost never $\xi < Q$

$$\mu \to \Delta^2 k$$

Note:

- If $\bar{k} > 0$, the motility is larger for large concentrations than for low concentrations.

Assume a Poisson distribution[6] with mean $\bar{N}$ for the number N of molecules in the measurement volume V, i.e. at any given time there is a fixed probability that a molecule

[6] One could also take a binomial distribution with p the probability for the molecules to be in the measurement volume. In the limit $p \ll 1$ with the mean number $\bar{N} = p\mathcal{N}$ of molecules inside V fixed (i.e. for very large total number $\mathcal{N}$ of molecules) the binomial distribution becomes a Poisson distribution.

$$\begin{aligned} P(N;\mathcal{N}) &= \binom{\mathcal{N}}{N} p^N (1-p)^{\mathcal{N}-N} = \\ &= \frac{\mathcal{N}!}{N!(\mathcal{N}-N)!}\left(\frac{\bar{N}}{\mathcal{N}}\right)^N \left(1-\frac{\bar{N}}{\mathcal{N}}\right)^{\mathcal{N}-N} = \\ &\underbrace{=}_{\mathcal{N}\to\infty} \frac{1}{N!}\underbrace{\frac{\mathcal{N}(\mathcal{N}-1)\ldots(\mathcal{N}-N+1)}{\mathcal{N}^N}}_{\to 1}\bar{N}^N \underbrace{\left(1-\frac{\bar{N}}{\mathcal{N}}\right)^{\mathcal{N}}}_{\to e^{-\mu}}\underbrace{\left(1-\frac{\bar{N}}{\mathcal{N}}\right)^{-N}}_{\to 1} \\ &= \frac{1}{N!}\bar{N}^N e^{-\bar{N}}. \end{aligned}$$

arrives (and then leaves) in V. The arrival times of different molecules are thus assumed to be independent of each other.

$$P(N;\bar{N}) = \frac{1}{N!}\bar{N}^N e^{-\bar{N}} \qquad N = \xi V \qquad \bar{N} = cV.$$

Transforming from ξ to N

$$\int F(\xi;c)d\xi = \int P(N;\bar{N})dN \to \sum_N P(N;\bar{N})$$

$$\mu = \Delta^2 k \left\{ 1 - \bar{k} \sum_{N=0}^{N^*} \frac{1}{N!} (cV)^N e^{-cV} \right\}$$

with $N^* = QV$. For χ we need $\mu'(c)$

$$\begin{aligned}
\mu'(c) &= -\Delta^2 k\bar{k} \left\{ \sum_{N=1}^{N^*} \underbrace{\frac{1}{N!} N (cV)^{N-1} V}_{\frac{1}{(N-1)!}c^{N-1}V^N} e^{-cV} + \sum_{N=0}^{N^*} \underbrace{\frac{1}{N!} (cV)^N (-V)}_{-\frac{1}{N!}c^N V^{N+1}} e^{-cV} \right\} \\
&= -\Delta^2 k\bar{k} e^{-cV} \left\{ \sum_{N=0}^{N^*-1} \frac{1}{N!} c^N V^{N+1} - \sum_{N=0}^{N^*} \frac{1}{N!} c^N V^{N+1} \right\} \\
&= \Delta^2 k\bar{k} e^{-cV} \frac{1}{N^*!} V (cV)^{N^*}
\end{aligned}$$

For large enough N^* approximate the factorial with Stirling's formula

$$\ln N! \approx N \ln N - N + \frac{1}{2}\ln(2\pi N) \qquad \Rightarrow \qquad N! \approx N^N e^{-N} (2\pi N)^{\frac{1}{2}} = (2\pi N)^{\frac{1}{2}} \left(\frac{N}{e}\right)^N$$

Together this yields

$$\chi \approx (\alpha - 1)\Delta^2 k\bar{k} V \frac{1}{\sqrt{2\pi N^*}} e^{-cV} \left(\frac{cVe}{N^*}\right)^{N^*}$$

Thus

$$\chi \to 0 \qquad \text{for } c \to 0$$
$$\chi \to 0 \qquad \text{for } c \to \infty$$

Maximal chemotaxis obtained for

$$0 = \frac{d}{dc}\left(e^{-cV} c^{N^*}\right) = \left(-V + N^* \frac{1}{c}\right) c^{N^*} e^{-cV} \qquad \Rightarrow \qquad c = \frac{N^*}{V}$$

Notes:

- For large and for small concentrations this model yields very poor chemotaxis.

- Optimal sensitivity is obtained for concentrations close to the threshold Q for switching.
- Expect quite generally that the motility reaches a plateau for large concentration $\Rightarrow$ chemotaxis will be weak at high concentrations in any system for which $\chi \propto \mu'$.
- The functionality could be increased if the threshold Q depended on the overall concentration in recent history, i.e. if the system **adapted** to the current environment.

This model:

- the chemotactic coefficient is proportional to the concentration-dependence of the motility
$$\chi \propto \frac{d\mu}{dc}.$$
- the step size is fixed and only the frequency depends on the concentration.

Keller and Segel also investigate a model in which the frequency is fixed, but the step size depends on concentration. Then one gets a different chemotactic coefficient, but it still satisfies (cf. Homework problem)
$$\chi \propto \frac{d\mu}{dc}.$$

In terms of the biochemical mechanism controling the motion these two systems are most likely very different, but they still lead to similar results.

However, when both, the step size and the frequency, depend on concentration, χ is not proportional to μ' any more; an additional cross-term arises (essentially a straightforward extension of the homework problem).

$\Rightarrow$ experimental comparisons of μ and χ would be able to provide insight into the mechanism.

1.3 Modeling Wave Propagation[7]

Having a model for the chemotactic motion of a population of bacteria, how can the formation of propagating bands in Adler's experiments be understood?

Key element:

- The bacteria consume food (glucose, galactose, amino acids) and in the aerobic case also oxygen.

Note:

- In general chemotaxis is not based on a metabolic signal, the signaling molecules are not used metabolically (i.e. they are not 'eaten').

[7](Keller and Segel, 1971b)

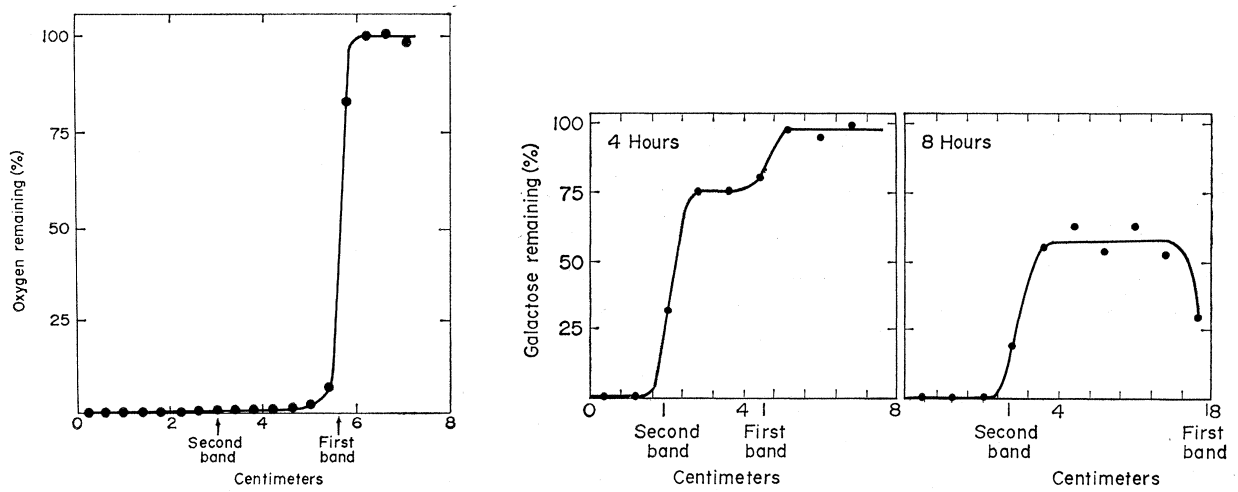

Figure 7: As the bacterial wave propagates they consume oxygen and galactose (Adler, 1966a)

Extend the equation for the chemotactic motion

- introduce an equation for the food s ('substrate')
- assume the substrate itself provides the information for the chemotaxis

$$\frac{\partial b}{\partial t} = \frac{\partial}{\partial x}\left[\mu(s)\frac{\partial b}{\partial x}\right] - \frac{\partial}{\partial x}\left[\chi(s)\, b\, \frac{\partial s}{\partial x}\right] \tag{2}$$

$$\frac{\partial s}{\partial t} = -K(s)\, b + D\frac{\partial^2 s}{\partial x^2} \tag{3}$$

Notes:

- The size of the bacteria population is constant:
  the equation has the form
  $$\frac{\partial b}{\partial t} = \frac{\partial}{\partial x} J$$
  therefore
  $$\frac{d}{dt}\int b dx = \int J\, dx = J|_{\text{boundaries}}$$
  For no-flux conditions no bacteria leave or enter the domain.
- Food consumption:
  - For low food concentrations the decay should be proportional to s since the chance of a bacterium to find the food molecules would be proportional to their density and the decay of s would be exponential.

– For high food concentrations the food consumption could be limited by the ability of the bacteria to absorb or metabolize it and K could go to a constant,

$$K(s) \to k$$

which would lead to a linear decay (for constant b).

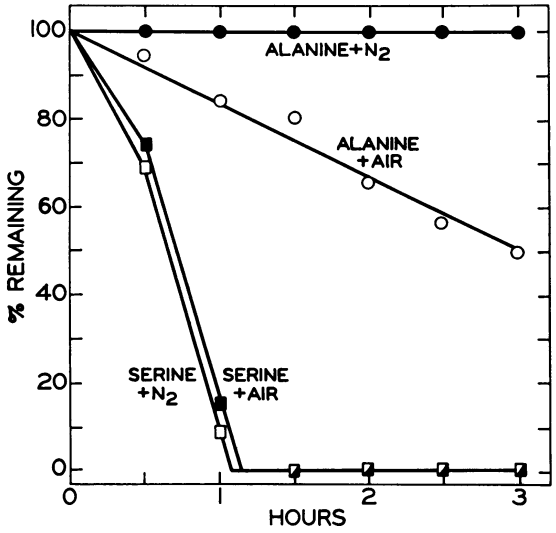

Figure 8: The experiments show linear rather than exponential decrease in food concentration (Adler, 1966b).

- Motility: in the absence of reliable data (when that paper was written), it is reasonable to assume that the motility of the bacteria is constant,

$$\mu = const.$$

While the dependence of the run frequency on the concentration is key for chemotactic response, the dependence of the diffusion coefficient on the concentration may amount to a higher-order effect.

- Substrate diffusion: the motility is significantly larger than diffusion coefficients for typical substrates $\Rightarrow$ for simplicity set

$$D = 0$$

- Chemotactic coefficient: in the simple model discussed in Sec.1.2 assuming constant motility μ would imply $\chi = 0$. When step size and step frequency are both concentration dependent, other relations between μ and χ are possible. Consider such a more general case.
Assuming

$$\chi(x) \propto s^{\alpha}$$

Keller and Segel show that within the model (2,3) with such a simple dependence on s no steadily propagating waves can be found unless $\alpha \leq -1$, i.e. χ becomes

singular for small s.
They argue that the chemotactic flux

$$\frac{1}{s}\frac{\partial s}{\partial x}$$

would then be consistent with the Weber-Fechner law of psychophysics, which expresses the observation that in many situations the sensation of a stimulus depends on the relative rather than the absolute change in that stimulus.
Therefore they assume

$$\chi(s) = \delta\,\frac{1}{s}.$$

In general, (2,3) need boundary conditions at both ends of the system (i.e. the tube). For closed ends these conditions would be Neumann conditions at both sides

$$\frac{\partial s}{\partial x} = 0 = \frac{\partial b}{\partial x}$$

The tube is thin, i.e. its aspect ratio is large $\Rightarrow$

- consider the tube to be infinitely long
- we can assume that the bands are propagating with a constant speed (cf. Fig.3).

Traveling-wave ansatz

$$b(x,t) = b(\xi) \qquad s(x,t) = s(\xi) \qquad \text{with} \quad \xi = x - ct$$

with the *yet unknown* wave speed c. Then (2,3) become, using also the simplification $D = 0$,

$$-c\frac{db}{d\xi} = \mu\frac{d^2b}{d\xi^2} - \frac{d}{d\xi}\left[\delta\,\frac{1}{s}b\frac{ds}{d\xi}\right] \tag{4}$$

$$-c\frac{ds}{d\xi} = -kb \tag{5}$$

Now the differential equation in s is only first order and we can only apply a single boundary condition for s. The equation for b is still second order and needs 2 boundary conditions. Where and what?

As the wave propagates the bacteria eat the food and the state behind the wave depends on the wave and cannot be imposed from outside. In contrast, the conditions ahead of the bands can be imposed:

- Ahead of the front the food concentration is still the initial concentration,

$$s \to s_\infty \qquad \text{for } \xi \to +\infty \tag{6}$$

- Ahead of the front there are no bacteria and therefore also their gradient vanishes,

$$b \to 0 \qquad \frac{db}{d\xi} \to 0 \qquad \text{for } \xi \to +\infty. \tag{7}$$

In (4) b and s have the same highest derivative $\Rightarrow$ possibly there is an algebraic connection between them. In contrast, solving first (5) would lead to the antiderivative of b. Therefore consider first (4). It can be integrated once directly

$$cb = -\mu\frac{db}{d\xi} + \delta\frac{1}{s}\frac{ds}{d\xi}b + C$$

Using the boundary condition (7) yields $C = 0$,

$$\frac{db}{d\xi} + \frac{1}{\mu}\left(c - \delta\frac{d}{d\xi}\ln s\right)b = 0$$

$$e^{\frac{c}{\mu}\xi - \frac{\delta}{\mu}\ln s}b = C_0$$

$$b = C_0 e^{-\frac{c}{\mu}\xi}\left(s\left(\xi\right)\right)^{\frac{\delta}{\mu}} \tag{8}$$

Inserted into (5) for s we get

$$\frac{ds}{d\xi} = \frac{k}{c}C_0 e^{-\frac{c}{\mu}\xi}s(\xi)^{\frac{\delta}{\mu}}$$

$$\underbrace{\int \frac{ds}{s^{\frac{\delta}{\mu}}}}_{\frac{1}{1-\frac{\delta}{\mu}}s^{1-\frac{\delta}{\mu}}} = \frac{k}{c}C_0\frac{\mu}{c}e^{-\frac{c}{\mu}\xi} + C_1$$

$$s = \left[\frac{k}{c^2}\left(\mu - \delta\right)C_0 e^{-\frac{c}{\mu}\xi} + \hat{C}_1\right]^{\frac{\mu}{\mu-\delta}}$$

What about C_0? It defines the origin of ξ

$$C_0 e^{-\frac{c}{\mu}\xi} = e^{-\frac{c}{\mu}(\xi-\xi_0)} \quad \text{with} \quad C_0 = e^{\frac{c}{\mu}\xi_0}$$

Using the boundary condition (6)

$$s(\xi) = \left[\frac{k}{c^2}\left(\mu - \delta\right)e^{-\frac{c}{\mu}(\xi-\xi_0)} + s_\infty^{\frac{\mu-\delta}{\mu}}\right]^{\frac{\mu}{\mu-\delta}}.$$

We can now insert $s(\xi)$ into the expression (8) to get $b(\xi)$.

It looks as if s could diverge for $\xi \to -\infty$. If the exponential dominates we have for $\mu > \delta$

$$s(\xi) \sim \left(e^{-\frac{c}{\mu}\xi}\right)^{\frac{\mu}{\mu-\delta}} = e^{-\frac{c}{\mu-\delta}\xi} \to \infty \quad \text{for} \quad \xi \to -\infty.$$

For s to be bounded, we therefore need

$$\delta > \mu.$$

In that case

$$s(\xi) \to 0 \qquad \text{for} \quad \xi \to -\infty$$

$$b(\xi) \sim e^{-\frac{c}{\mu}\xi}\left(e^{-\frac{c}{\mu-\delta}\xi}\right)^{\frac{\delta}{\mu}} = e^{-\frac{c\mu}{\mu(\mu-\delta)}\xi} \to 0 \qquad \text{for} \quad \xi \to -\infty.$$

Thus, within the model, as the band propagates into the fresh medium

- the bacteria consume all of the food
- no bacteria are 'left behind'.

Now we have a solution, but still do not know the wave speed c. How do we get that? What information have we not used yet?

We have used the initial substrate concentration. However, the total size of the bacteria population, which is constant in time, has not entered the equations yet. Integate (5) over the whole domain,

$$\int_{-\infty}^{\infty} b\,dx = \frac{c}{k}\left(s(+\infty) - s(-\infty)\right) = \frac{c}{k} s_\infty$$

This equation determines the wave speed c.

Notes:

- The model therefore predicts that the wave speed grows (linearly) with the total population size and decreases with the concentration of the food. Not clear whether these predictions have been tested.
- To check whether ignoring the diffusion of s is justified we need to look at $D\frac{d^2s}{d\xi^2}/kb$. From the solutions one can show with some algebra that this ratio is proportional to D/μ, i.e. it can be ignored if the diffusion is weak compared to the motility.

The model captures the traveling bands if $\chi(s) \propto s^{-1}$. How does this compare with experiments? The flux of bacteria is given by

$$J(x) = -\mu\frac{\partial b}{\partial x} + b\,\chi(s)\frac{\partial s}{\partial x} = -\mu\frac{\partial b}{\partial x} + b\,\frac{\partial}{\partial x}\ln s$$

Subsequent experiments with well-controled profiles $s(x)$ show

- For a linear concentration profile the bacteria pile up on the ramp $\Rightarrow$ the flux of bacteria is not x-independent
  $\Rightarrow \chi$ must depend on s
- For an exponential concentration profile the bacterial flux is quite close to x-independent: the pile-up occurs at the end of the ramp.

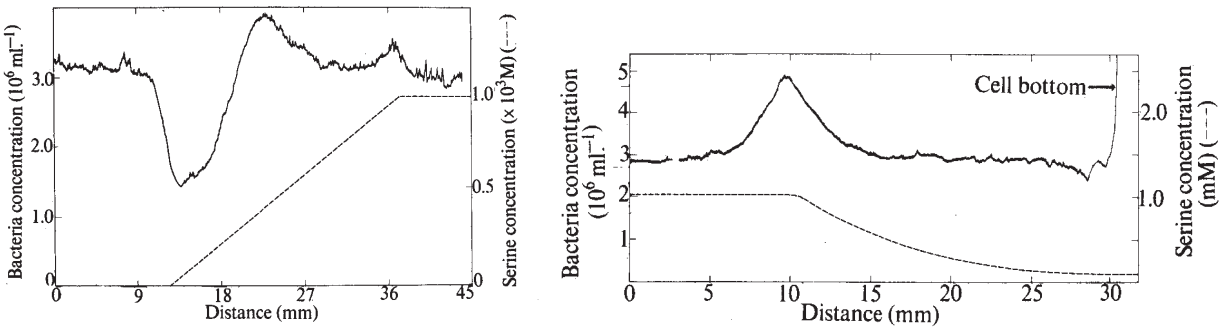

Figure 9: a) For a linear profile of $s(x)$ the bacteria pile up on the ramp. b) For an exponential profile the bacteria concentration is quite constant on the ramp. (Dahlquis et al., 1972)

- The accumulation at the end of the ramp grows linearly in time, giving a measure of the flux along the ramp.
- The flux depends on the overall concentration (as measured by the plateau concentration) $\Rightarrow$ dependence of $\chi(s)$ on s is modulated in addition by s.

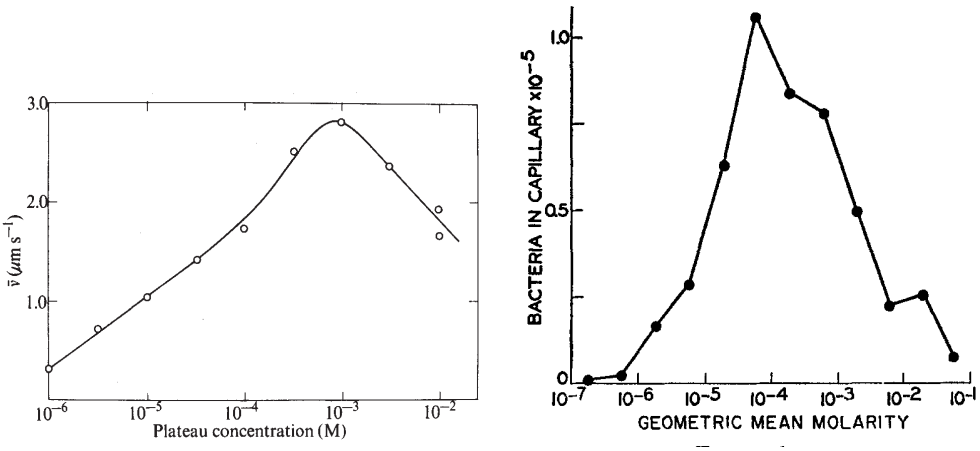

Figure 10: a) The flux along the exponential ramp depends on the overall concentration (Dahlquis et al., 1972). b) For fixed concentration ratio (inside vs outside of capillary) the accumulation of bacteria in the capillary is maximal at intermediate concentrations (Mesibov et al., 1973).

Lapidus and Schiller (Lapidus and Schiller, 1976) introduce a sensitivity function instead of δ

$$J = b\,\hat{\delta}\frac{\partial}{\partial x}\frac{s}{s+k} = b\,\hat{\delta}\,\frac{ks}{(s+k)^2}\frac{\partial}{\partial x}\ln s \qquad \delta = \hat{\delta}\frac{ks}{(s+k)^2} \tag{9}$$

and compare with the experiments in (Dahlquis et al., 1972).

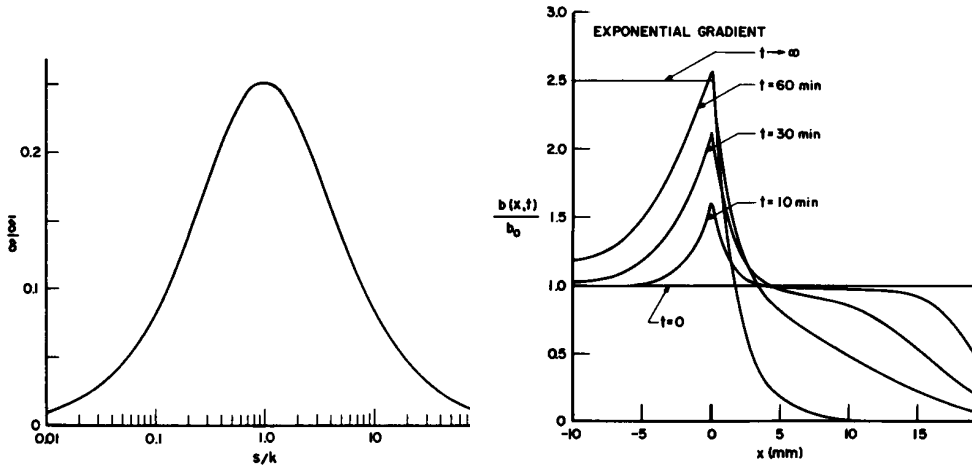

Figure 11: a) Sensitivity function δ of (9). b) Simulations with exponential gradients. During early times (up $t = 10$min) the concentration is quite constant on the exponential ramp (Lapidus and Schiller, 1976).

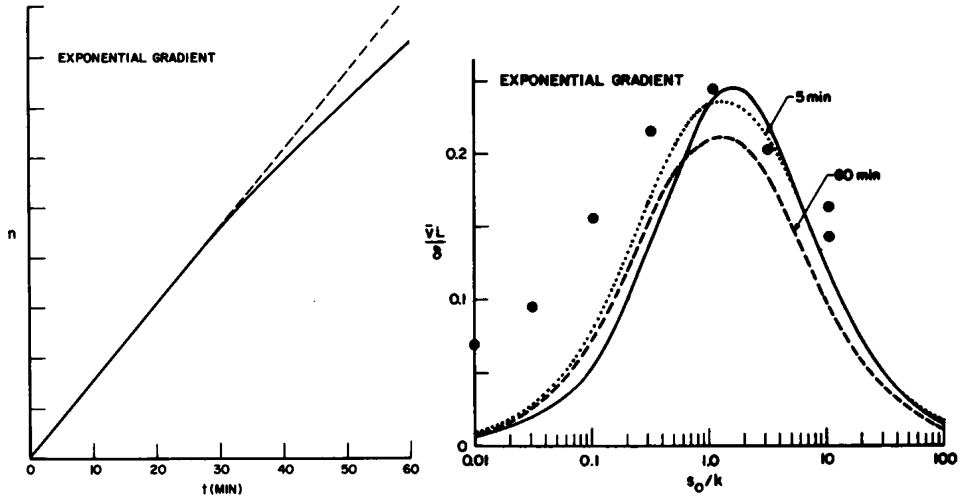

Figure 12: a) Linear growth of the accumulation in the simulation of (Lapidus and Schiller, 1976). b) Dependence of the simulated flux on the concentration in the exponential ramp configuration agrees qualitatively with experiments (solid circles) (Lapidus and Schiller, 1976).

1.4 Sensing the Chemoattractant[8]

How does the bacterium know which way to go? It seems that it needs to measure spatial concentration gradients. How well can it measure concentrations in the first place? To measure concentrations one has to count the number of molecules at the sensor. That number fluctuates. What kind of limits does this set (Berg and Purcell, 1977)?

Consider a chemosensor that counts the number of molecules n in a small volume of size a^3. On average, that will be

$$\langle n \rangle = c\, a^3.$$

At any given moment in time the number of molecules is likely to deviate from $\langle n \rangle$, the measurement is noisy. We expect the standard deviation σ in the measurements to be of order $\sqrt{\langle n \rangle}$. Why?

Consider the small measurement volume to be part of a large volume V that contains N molecules of the chemoattractant. Assume that at any given time each molecule has equal probability

$$p = \frac{a^3}{V}$$

to be in the measurement volume. If these molecules are independent of each other, then the probability to have exactly n molecules in the measurement volume is given by the binomial distribution

$$P(n; N) = \left(\begin{array}{c} N \\ n \end{array} \right) p^n q^{N-n} \qquad \text{with} \quad q = 1 - p.$$

[8] worthwhile video by H. Berg: https://www.youtube.com/watch?v=ioA1yuIA-t8

Then

$$\langle n\rangle = \sum_{n=0}^{N} n \left(\begin{array}{c} N \\ n \end{array} \right) p^n q^{n-n} = p\frac{\partial}{\partial p} \sum_{n=0}^{N} \left(\begin{array}{c} N \\ n \end{array} \right) p^n q^{N-n} = p\frac{\partial}{\partial p} (p+q)^N = pN = \frac{a^3}{V}\, cV = c\, a^3$$

as expected.

The variance is then given by

$$\begin{aligned} \sigma^2 &= \langle n^2\rangle - \langle n\rangle^2 = p\frac{\partial}{\partial p}\left(p\frac{\partial}{\partial p} \sum_{n=0}^{N} \left(\begin{array}{c} N \\ n \end{array} \right) p^n q^{N-n} \right) - (pN)^2 = \\ &= p\frac{\partial}{\partial p}\left(p\frac{\partial}{\partial p}(p+q)^N \right) - (pN)^2 = \\ &= p\frac{\partial}{\partial p}\left(Np(p+q)^{N-1} \right) - (pN)^2 = \\ &= pN(p+q)^{N-1} + Np^2(n-1)(p+q)^{N-2} - (pN)^2 = \\ &= pN - p^2N = Npq \end{aligned}$$

The relative error in the measurement of the concentration is therefore

$$\frac{\delta c}{c} = \frac{\sigma}{\langle n\rangle} = \frac{\sqrt{Npq}}{pN} = \sqrt{q}\,\frac{1}{\sqrt{pN}} = \sqrt{q}\,\frac{1}{\sqrt{\langle n\rangle}} \underbrace{\sim}_{a^3 \ll V \;\; q\to 1} \frac{1}{\sqrt{\langle n\rangle}} = \frac{1}{\sqrt{ca^3}}.$$

For small measurement volumes the relative error is therefore quite large.

To improve the measurement, the bacterium could measure K times.

Central Limit Theorem:
If $\{x_1, x_2, \ldots, x_K\}$ are K *independent* and identically distributed random variables drawn from a distribution with expected value μ and finite variance σ^2, then

$$\frac{1}{K}\sum_{i=1}^{K} x_i - \mu \xrightarrow{\mathsf{d}} \mathcal{N}\left(0, \frac{\sigma^2}{K}\right),$$

i.e. the sample means converge to μ and they are normally distributed with a variance $\frac{\sigma^2}{N}$.

But: the molecules enter and leave the measurement volume by local diffusion $\Rightarrow$ it takes some time for the number of molecules in a^3 to change. The distributions will be correlated for some correlation time τ_c . By dimensional analysis we expect

$$\tau_c = \frac{a^2}{D}$$

with D being the diffusion coefficient.

If the bacterium averages the measurements over a time τ_{avg}, it can only take $K = \frac{\tau_{avg}}{\tau_c}$ *independent* measurements

$$\left.\frac{\delta c}{c}\right|_{\tau_{avg}} = \frac{1}{\sqrt{K}}\frac{1}{\sqrt{ca^3}} = \sqrt{\frac{\tau_c}{\tau_{avg}}}\frac{1}{\sqrt{ca^3}} = \frac{1}{\sqrt{Dac\tau_{avg}}}.$$

To resolve a relative concentration difference $\frac{\delta c}{c}$ the bacteria has to measure for a duration of

$$\tau_{avg} = \frac{1}{D\,a\,c}\left(\frac{c}{\delta c}\right)^2 .$$

Could a bacterium sense the concentration difference across its body reliably within a reasonable time?[9] Consider the experiment of Fig.10, which uses concentration gradients that are well above the sensitivity of the bacterium.

- Absolute concentrations in (Dahlquis et al., 1972) for which the bacteria still reliably perform chemotaxis are as low as 10^{-6}M

$$c \sim 10^{-6}\text{Mol} \sim 10^{-6} \times 6 \cdot 10^{23} \frac{1}{10^3\text{cm}^3} = 6 \cdot 10^{14} \frac{1}{\text{cm}^3}$$

- Size of the bacterium

$$a \sim 1\mu\text{m} = 10^{-4}\text{cm}$$

- Diffusion of the chemoattractant

$$D \sim 10^{-5} \frac{\text{cm}^2}{s}$$

- Relative concentration difference across the bacterium (in the experiment of Dahlquis et al. (1972) the concentration goes from essentially 0 to its full value in about 1cm)

$$\frac{\delta c}{c} = \frac{1}{c}\frac{dc}{dx}\,a \sim \frac{1}{\text{cm}} 10^{-4}\,\text{cm} = 10^{-4}$$

To resolve such a gradient at this low concentration the bacterium would have to measure for a duration of

$$\tau_{avg} \sim \frac{1}{10^{-5}10^{-4}6 \cdot 10^{14}} \left(10^4\right)^2 \frac{\text{s}\,\text{cm}^3}{\text{cm}^2\,\text{cm}} \sim 10^3\,\text{s} \sim 20\,\text{minutes}$$

This time is way too long; the bacterium needs to decide faster than that to ever get to its food. Only at the optimal concentration of 10^{-3}M (Fig.10) the bacterium could get a sufficiently accurate measurement within 1 second.

To increase the precision or reduce the sampling time for a given concentration the bacterium can

- increase the receptor size
  limited by the size of the bacterium
- increase the diffusion coefficient
  the bacterium cannot really change the diffusion coefficient. One could imagine that it could stir up the fluid and enhance the exchange that way.

Thus

[9] Web site to find numbers relevant in biology: http://bionumbers.hms.harvard.edu/default.aspx

- The method that bacteria use for chemotaxis cannot rely on spatial gradients across their body.
- This limitation reflects the discrete nature of the chemoattractant molecules and the small size of the bacterium, which limits the receptor size as well as the distance across which differences would have to be measured. Improving the sensor quality will not overcome this limitation.

To be exposed to larger difference in concentration the bacteria can swim around:

- with a swimming velocity of $10 - 20\mu$m/s they can cover $10 - 20\mu$m within 1 second, which increases the concentration difference by a factor of 10-20. Even for the very low concentration of 10^{-6}M the required time for averaging is then of the order

  $$\tau_{avg}/10^2 \ldots \tau_{avg}/20^2 \sim 2 \ldots 10\,\mathrm{s}$$

  which is closer to a reasonable range.

So, what do bacteria do?

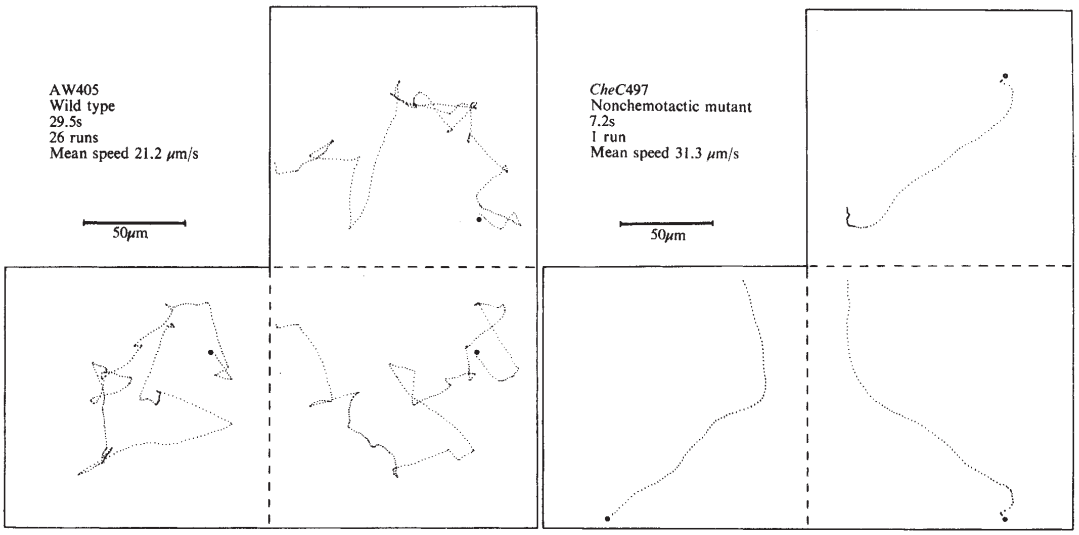

Figure 13: Three-dimensional trajectories of E. coli bacteria in a homogeneous solution. a) Chemotactic wildtype. b) Non-chemotactic mutant (Berg and Brown, 1972).

Even for spatially homogeneous concentrations of the chemoattractant the chemotatic bacteria perform run-and-tumble motion with the direction of the runs changing randomly during the tumbles. The non-chemotactic mutants tumble only very rarely and perform mostly runs.

The durations of the runs and of the tumbles are exponentially distributed, i.e. they follow a Poisson statistics, implying that at any given time during the run (tumble) there is a finite probability that the run (tumble) stops.

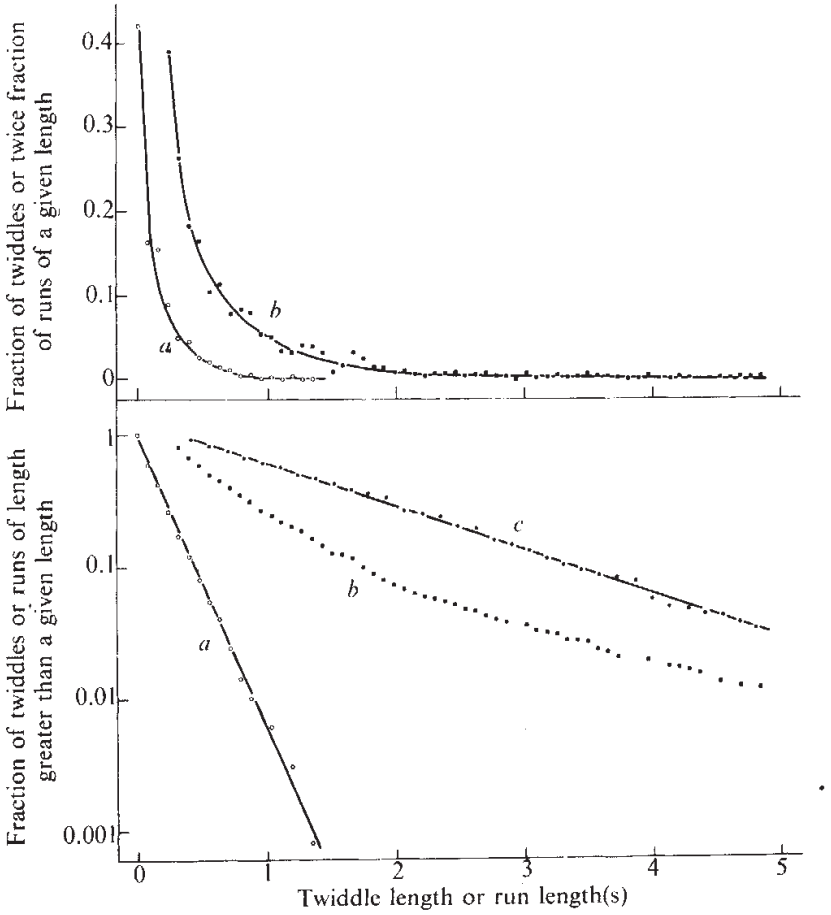

Figure 14: Runs and tumbles satisfy Poisson statistics. The plot on the bottom shows the data from the graph on the top on a logarithmic scale. Cumulative distribution for tumbles (curve *a*) and runs (curve *b*) that are longer than the indicated duration (Berg and Brown, 1972).

In the presence of gradients (Berg and Brown, 1972)

- the mean duration of runs *down* the gradient is unchanged compared to that in homogeneous concentrations
- the mean duration of runs *up* the gradient is twice as as long

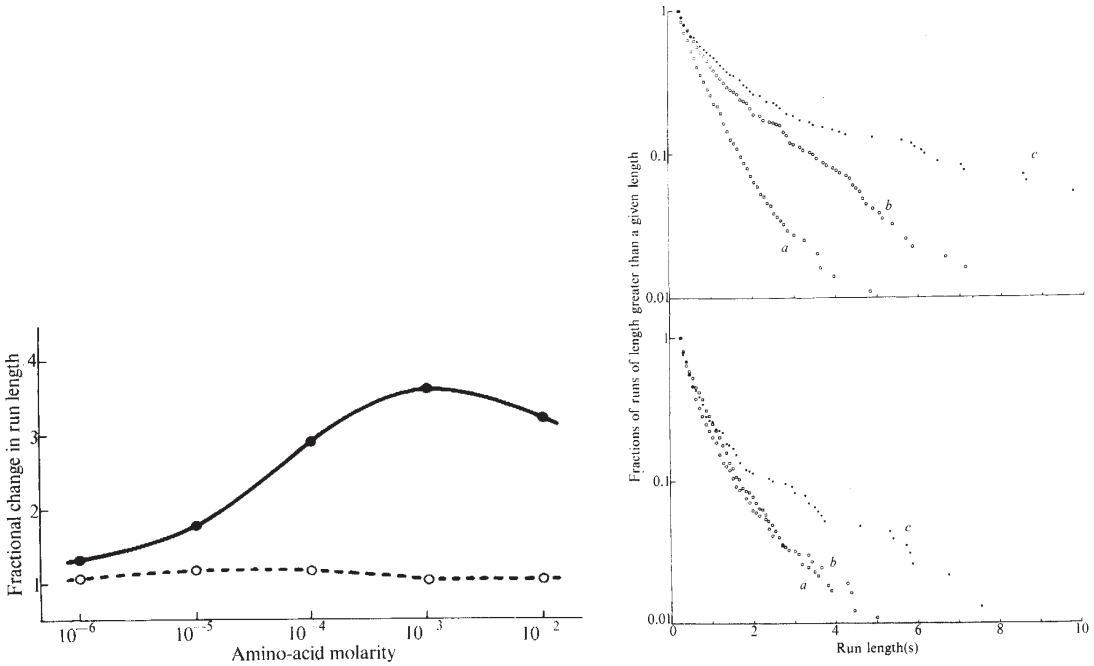

Table 3 Analysis of Runs which Move the Bacteria Up the Gradient or Down the Gradient

Attractant	Serine	Serine	Aspartate	Aspartate
Net displacement of runs	Up	Down	Up	Down
Mean concentration (μM)	10.0±2.8	9.2±2.6	8.8±1.9	8.1±1.9
Mean run length (s)	2.19±3.43	1.40±1.88	1.07±1.80	0.80±1.38
Mean run length expected from the control run length (Table 2) and the concentration dependence (Fig. 5) (s)	1.48	1.45	0.82	0.82

Figure 15: Run durations. a) Dependence on the concentration of the spatially homogeneous solution (scaled by the run length without chemoattractant). b) Cumulative distributions of run lengths in serine (top) and aspartate (bottom) experiments (a=control, b=down the gradient, c=up the gradient). c) Quantitative comparison (Berg and Brown, 1972).

How do the runs and tumbles come about?

The bacteria are propelled by a bundle of flagella at one of the body that are rotated by a molecular motor (cf. Fig.5).

- Counter-clockwise rotation:
  - the flagella in the bundle align with each other and rotate together ⇒ strong propelling force forward ⇒ run
  - attractants induce CCW rotation (Larsen et al., 1974)
- Clockwise rotation:

  - the flagella become disorganized and the bacterium performs random rotation $\Rightarrow$ tumble.
  - repellents induce CW rotation (Larsen et al., 1974)

Notes:

- With the run lengths being on the order of a few seconds the bacteria are operating quite close to the limit imposed by the fluctuations in the concentration.
- The run lengths are also limited by the fact that the bacteria cannot swim perfectly straight; their orientation fluctuates leading to rotational diffusion. Thus, after some time the run may not go in the direction of increasing concentration any more. Then the bacteria need to measure again.
- How can the motor so *sensitively* be switched between different directions of rotation?

If the bacterium measures and compares concentrations by moving about, does it actually compare concentrations in *time*?

Response to spatially homogeneous, temporally varying concentrations of an attractant (Macnab and Koshland, 1972):

- Sudden strong increase $\Rightarrow$ transient increase in runs. The velocities relax back to the control within few minutes.
- Sudden strong decrease $\Rightarrow$ transient increase in tumbles. The velocities relax back to the control values after ~ 10s.

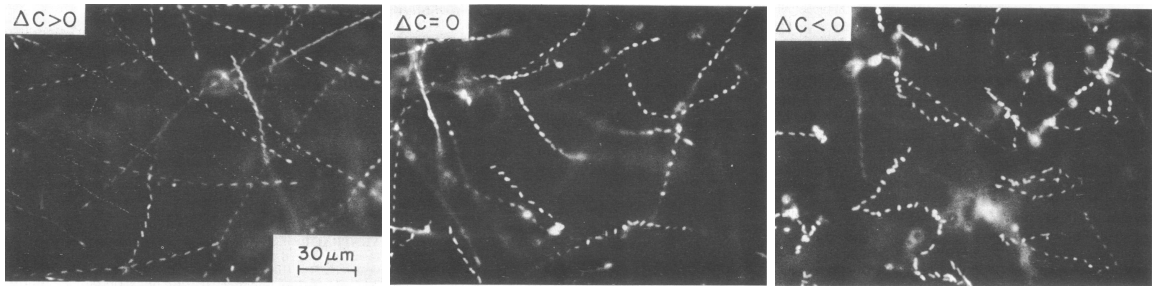

Figure 16: Trajectories of *S. typhimurium* after sudden large, spatially homogeneous changes in the concentration of an attractant. a) A temporal increase in concentration leads to more long runs. b) Constant concentration control. c) A decrease leads to increased tumbling. (Macnab and Koshland, 1972)

More refined experiments with small, well-controled temporal gradients show (Brown and Berg, 1974)

- for increasing concentrations

  - the mean length of runs depends on $\frac{dc}{dt}$ and c
  - With the large jumps in (Macnab and Koshland, 1972) the transients could last minutes, suggesting a long memory. The experiments with small changes suggest the memory must be less than 100s (Brown and Berg, 1974).

- for decreasing concentrations there is little effect on the run length

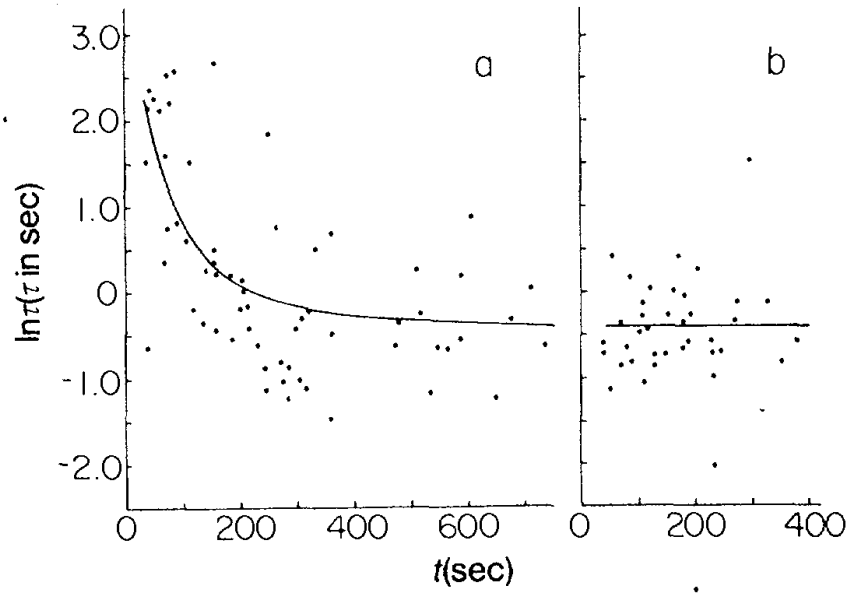

Figure 17: Dependence of mean run length on temporal gradient in the concentration. a) The temporal gradient of glutamate was produced by an enzymatic reaction $C(t) = C_e\left(1 - e^{-t/T}\right)$. Thus, the rate of change decreased exponentially with time. b) No temporal gradient (no enzyme included) (Brown and Berg, 1974).

Aspects of the dependence can be understood in terms of a chemoreceptor protein P that binds with the chemoattractant C to form a complex PC (Mesibov et al., 1973)

$$P + C \underbrace{\overbrace{\rightleftharpoons}^{k_1}}_{k_2} PC$$

$$\frac{d[P]}{dt} = -k_1[P][C] + k_2[PC]$$

If the reactions are fast compared to rate of change of the concentration one gets

$$\frac{[P][C]}{[PC]} = \frac{k_2}{k_1} \equiv K_D.$$

The total amount of the protein $[P_{tot}]$, i.e. the sum of the protein bound in $[PC]$ and the unbound protein $[P]$, is constant,

$$[P] = [P_{tot}] - [PC],$$

yielding

$$K_D = \frac{([P_{tot}] - [PC])\,[C]}{[PC]} = \frac{\left(1 - \frac{[PC]}{[P_{tot}]}\right)[C]}{\frac{[PC]}{[P_{tot}]}}$$

and

$$\frac{[PC]}{[P_{tot}]} = \frac{[C]}{K_D + [C]}$$

The temporal gradient in $[PC]$ is then

$$\frac{d}{dt}[PC] = \frac{K_D}{(K_D + [C])^2}\frac{d[C]}{dt}.$$

Brown and Berg find the best and very good fit of their run length data for

$$\langle \ln \tau \rangle = \ln \tau_0 + \alpha \frac{d[PC]}{dt}, \qquad \text{for} \quad \frac{d[C]}{dt} > 0.$$

Is this response to temporal gradients compatible with models that assume the response depends on spatial gradients?
If the bacteria swim in a fixed spatial concentration gradient with fixed speed, the spatial gradients translate into temporal gradients

$$\frac{d[C]}{dx} = v\frac{d[C]}{dt}.$$

The motor of the bacteria seems to have only two states: running and tumbling $\Rightarrow$ the swimming speed is presumably quite fixed during a run, making such a substitution a reasonable approximation. The sensitivity of the chemotaxis should then depend on

$$\frac{d}{dx}[PC] = \frac{K_D}{(K_D + [C])^2}\frac{d[C]}{dx} = \frac{K_D\,[C]}{(K_D + [C])^2}\left(\frac{1}{[C]}\frac{d[C]}{dx}\right). \tag{10}$$

In the experiments of Mesibov, Ordal, and Adler (Mesibov et al., 1973) (cf. Fig.10) on the accumulation of bacteria in the capillary the concentration ratio between the solution and the pipette was held constant as the overall concentration was changed, i.e. $\frac{1}{[C]}\frac{d[C]}{dx}$ was held fixed. The resulting accumulation of bacteria is quite consistent with (10). Compare also (10) with the sensitivity function (9) introduced by Lapidus and Schiller (Lapidus and Schiller, 1976).

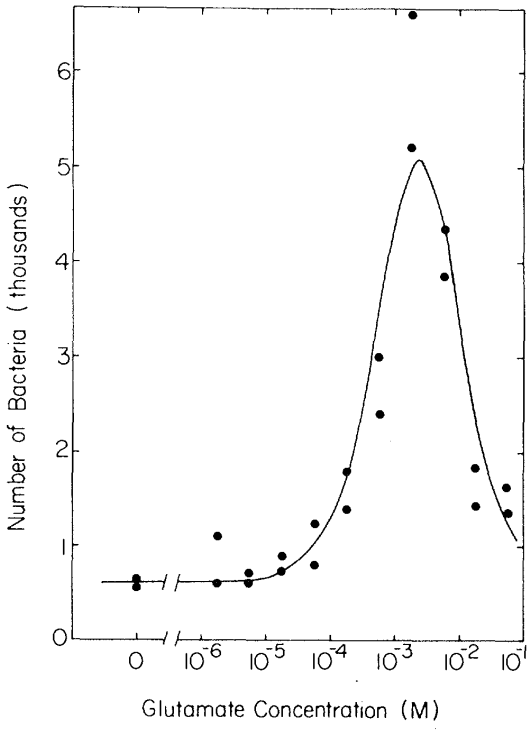

Figure 18: Sensitivity: dependence of the chemotactic accumulation of bacteria in the capillary on the concentration (cf. Fig.10). For all glutamate concentrations the initial concentration in the capillary was 3.16 times larger than in the suspension. The curve is a fit to $K_D[C]/(K_D+[C])^2$. (Brown and Berg, 1974).

In fact, Segel considered a model in which the switching of directions depends on the rate of change of the receptor response,

$$\begin{aligned}
\frac{\partial E^+}{\partial t} + \underbrace{\frac{\partial}{\partial x}\left(vE^+\right)}_{\text{advection}} &= \underbrace{k_{-1}C^+}_{\text{dissociation}} - \underbrace{k_1 s E^+}_{\text{binding of substrate}} + \underbrace{\sigma^- E^-}_{\text{left to right}} - \underbrace{\sigma^+ E^+}_{\text{right to left}} \\
\frac{\partial C^+}{\partial t} + \frac{\partial}{\partial x}\left(vC^+\right) &= -k_{-1}C^+ + k_1 s E^+ + \sigma^- C^- - \sigma^+ C^+ \\
\frac{\partial E^-}{\partial t} - \frac{\partial}{\partial x}\left(vE^-\right) &= k_{-1}C^- - k_1 s E^- - \sigma^- E^- + \sigma^+ E^+ \\
\frac{\partial C^-}{\partial t} - \frac{\partial}{\partial x}\left(vC^-\right) &= -k_{-1}C^- + k_1 s E^- - \sigma^- C^- + \sigma^+ C^+ .
\end{aligned}$$

Here $E^\pm$ is the concentration of bacteria that swim to the right/left and that have a receptor to which no substrate is bound. $C^\pm$ is the concentration of bacteria in which the substrate is bound to the receptor. $\sigma^\pm$ gives the switching rate between right and left runs. Since the run duration is found to depend on the rate of change of the concentration only if the concentration increases, Segel takes - considering the case $\frac{\partial s}{\partial x} > 0$ - for the switching rates $\sigma^\pm$

$$\sigma^+ = f\left(\left(\frac{\partial}{\partial t} + v\frac{\partial}{\partial x}\right)\frac{C^+}{E^+ + C^+}\right) \qquad \text{and} \qquad \sigma^- = f\left(0\right).$$

The concentration of the substrate is assumed to satisfy

$$\frac{\partial c}{\partial t} = -k_1 s \left(E^+ + E^-\right) + k_{-1}\left(C^+ + C^-\right) - d + D\frac{\partial^2 c}{\partial x^2},$$

i.e. the substrate is bound by the receptor, is degraded through a reaction that is limited by the availability of an enzyme (i.e. rates is independent of s) and diffuses. For this model Segel derived the chemotactic equation (1),

$$\frac{\partial b}{\partial t} = -\frac{\partial}{\partial x}\left(-\mu\frac{\partial b}{\partial x} + \chi b\frac{\partial c}{\partial x}\right),$$

recovering the form of the previous Keller-Segel model.

Note:

- The change in swimming is only transient $\Rightarrow$ the control of the flagellar motor must show **adaptation**, i.e. when the concentration goes up the control system must be adjusting itself to that new 'normal'.
- Chemotaxis operates over a wide range of concentration: the **dynamic range** of the adaptation must be large.

implies that saturation effects are not important in the enzyme experiments.

The capillary assays were done by Susan MacFadden. This work was supported by a grant from the National Science Foundation (GB-30337).

1. Engelmann, T. W. (1883) *Pflügers Arch. Gesamte Physiol. Menschen Tiere* **30,** 95–124.
2. Metzner, P. (1920) *Jahrb. Wiss. Bot.* **59,** 325–412.

Figure 19: Side remark: it is not always clear how authorship for a paper was decided (Brown and Berg, 1974).

1.5 Robust Adaptation

Understanding chemotaxis in E. coli is important in itself. In addition, it provides an excellent model system to study signal transduction more generally; results obtained for the chemosensory pathway E. coli are most likely also relevant in other animals and for other senses.

Need facts first:[10]

- Motor control via CheY
  - when it is phosphorylated by CheA, it makes the flagella motors turn clockwise, which makes the bacterium tumble
  - the phosphorylated state CheY-P is relatively stable on its own ($\mathcal{O}(10\text{s})$), which is too long for the bacterium to tumble $\Rightarrow$ it becomes dephosphorylated by CheZ, which makes the tumbling periods less than 1s.
- Receptor complex
  - consists of the receptor, CheW, and CheA
  - binds the ligand (chemoattractant)
  - can be in an active and an inactive state
    - when it is in the active state the kinase CheA phosphorylates CheY
  - has multiple methylation sites, i.e. sites at which CH_3 can be added
    - methylation is performed by CheR
    - demethylation by CheB; it is enhanced if CheB is phosphorylated by CheA.
  - the probability of the complex to be active
    - decreases when a chemoattractant is bound to it
    - increases with methylation

The methylation of the receptor complex provides a feedback loop, which reduces the impact of the ligand on the activity level of CheA.

[10] Good video by H. Berg https://www.ibiology.org/biophysics/bacterial-motion/#part-2

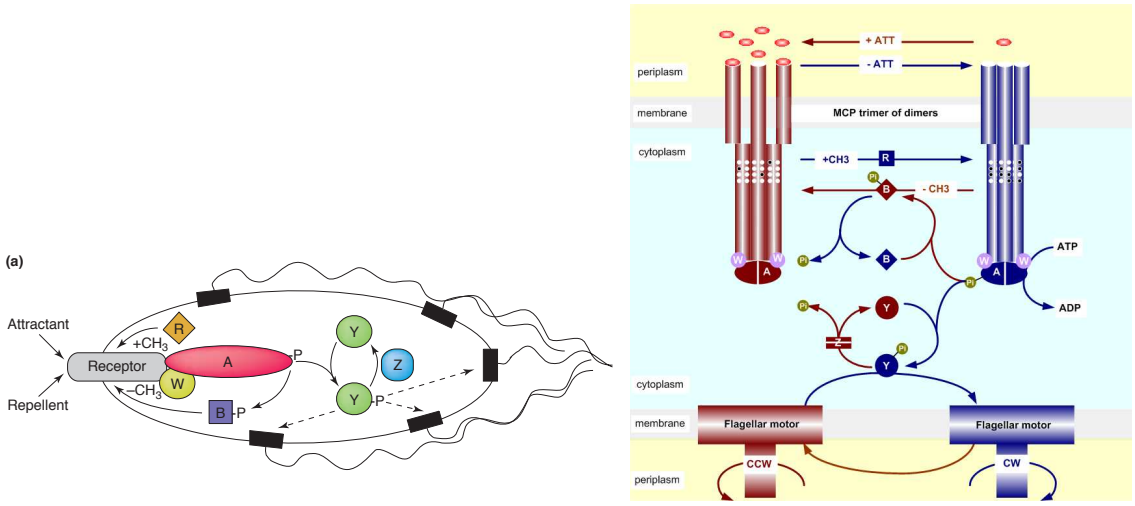

Figure 20: Sketch of the signal transduction pathway (Sourjik, 2004; Othmer et al., 2013)

Consider the reaction scheme of Fig.21 (Alon, 2007).

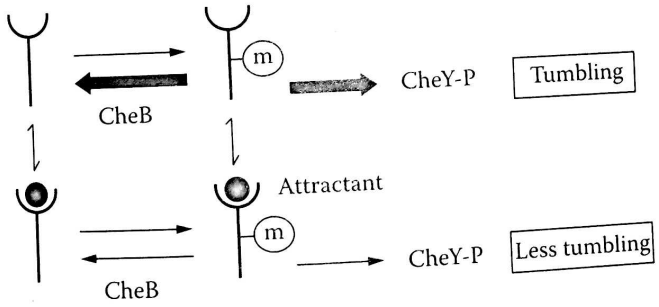

Figure 21: Reaction scheme of the model for fine-tuned adaptation(Alon, 2007).

The receptor complex X can be in 4 different states

- unmethylated without attractant X_{00}: inactive
- unmethylated with attractant X_{0a}: inactive
- methylated without attractant X_{m0}: strongly active a_0
- methylated with attractant X_{ma}: weakly active $a_1 < a_0$.

Reactions:

- Attractant binding

$$X_{00} + L \underbrace{\overset{V_L^+}{\underset{V_L^-}{\rightleftarrows}}} X_{0a}$$

$$X_{m0} + L \underbrace{\overbrace{\rightleftarrows}^{V_L^+}}_{V_L^-} X_{ma}$$

For simplicity we take the ligand binding rates the same for the methylated and unmethylated receptor.

- Methylation by CheR and demethylation by CheB

$$X_{00} + CH_3 \underbrace{\overbrace{\rightleftarrows}^{V_R R}}_{V_{B0} B} X_{m0}$$

$$X_{0a} + CH_3 \underbrace{\overbrace{\rightleftarrows}^{V_R R}}_{V_{Ba} B} X_{ma}$$

The goal of the adaptation is for the activity in *steady state* to be independent of the concentration L of the ligand (attractant),

$$A(L=0) = A(L).$$

The activity change should change only *transiently,* when the attractant becomes bound or unbound.

Only the pool of methylated receptors $\{X_{m0}, X_{ma}\}$ contributes to activity,

$$A = a_0 X_{m0} + a_1 X_{ma}.$$

When methylated receptors become bound to the attractant they become less active and the overall activity of that pool decreases. To keep the overall activity the same, the pool of methylated receptors needs to be increased $\Rightarrow$ the rate with which CheB demethylates the receptor should be smaller when the attractant is bound than when it is not bound

$$V_{Ba} < V_{B0}.$$

Evolution equations for the states without ligand (R and B are the concentrations of CheR and CheB and L is the concentration of the ligand)

$$\frac{dX_{00}}{dt} = -V_R R \frac{X_{00}}{K_0 + X_{00}} + V_{B0} B \frac{X_{m0}}{K + X_{m0}} + V_L^- X_{0a} - V_L^+ X_{00} L$$

$$\frac{dX_{m0}}{dt} = V_R R \frac{X_{00}}{K_0 + X_{00}} - V_{B0} B \frac{X_{m0}}{K + X_{m0}} + V_L^- X_{ma} - V_L^+ X_{m0} L$$

Analogously, for the states with ligand

$$\frac{dX_{0a}}{dt} = -V_R R \frac{X_{0a}}{K_a + X_{0a}} + V_{Ba} B \frac{X_{ma}}{K + X_{ma}} - V_L^- X_{0a} + V_L^+ X_{00} L$$

$$\frac{dX_{ma}}{dt} = V_R R \frac{X_{0a}}{K_a + X_{0a}} - V_{Ba} B \frac{X_{ma}}{K + X_{ma}} - V_L^- X_{ma} + V_L^+ X_{m0} L$$

Since the total amount of receptor is constant,

$$X_{00} + X_{m0} + X_{0a} + X_{Ma} = \text{const.},$$

we do not need to consider the equation for X_{m0}.

Consider only switching between two extreme situations:

- no attractant, $L = 0$, $X_{ma} \to 0$ and $X_{0a} \to 0$ since

$$\frac{d}{dt}\left(X_{0a} + X_{ma}\right) = -V_L^-\left(X_{0a} + X_{ma}\right)$$

- large concentration of attractant so that $X_{m0} \to 0$ and $X_{00} \to 0$

$$\frac{d}{dt}\left(X_{00} + X_{m0}\right) = -V_L^+ L\left(X_{00} + X_{m0}\right) + V_L^-\left(X_{0a} + X_{ma}\right)$$

When switching from $L = 0$ to L large:

- initially only X_{00} and X_{m0} are non-zero. Their relative size depends on V_R and $V_{B0}B$.
- immediately after switching they start to decay and feed into X_{0a} and X_{ma}. Because the attractant binds rapidly, the total size of the pool $\{X_{m0}, X_{ma}\}$ of methylated receptors stays the same, but the fraction of receptors bound to the attractant increases $\Rightarrow$ the activity decreases. The balance between X_{ma} and X_{0a} is initially determined by the balance of X_{m0} and X_{00}.
- on a longer time scale the slower methylation and demethylation processes kick in $\Rightarrow$ the balance between X_{ma} and X_{0a} will change in factor of X_{ma}, reflecting the reduced demethylation rate V_{Ba} compared to $V_{B0} \Rightarrow$ the size of the pool $\{X_{m0}, X_{ma}\}$ increases and with it the activity recovers.

The experiments show that the methylation by CheR is saturated: $X_{00} \gg K$. For simplicity, we take the Michaelis-Menten constants to be the same, $K_0 = K_a$.

To compare the steady states before and after applying an attractant, it is then sufficient to consider

$$V_R R = V_{B0} B \frac{X_{m0}}{K + X_{m0}} \qquad \text{for} \quad L = 0$$

$$V_R R = V_{Ba} B \frac{X_{ma}}{K + X_{ma}} \qquad \text{for} \quad L \neq 0 \text{ large}$$

This yields the steady-states

$$X_{m0} = \frac{K V_R R}{V_{B0} B - V_R R}$$

$$X_{ma} = \frac{K V_R R}{V_{Ba} B - V_R R}$$

For perfect adaptation

$$A(L=0) = A(L)$$

one needs therefore

$$\begin{aligned} a_0 X_{m0} &= a_1 X_{ma} \\ \frac{a_0}{V_{B0}B - V_R R} &= \frac{a_1}{V_{Ba}B - V_R R} \end{aligned} \tag{11}$$

Notes:

- In order for adaptation to occur, the parameters of the system have to satisfy a very specific condition. This would require that they be specifically tuned, which can be achieved by tuning
  - the methylation and demethylation rates V_{B0}, V_{Ba}, or V_R
  - the concentrations R and B of CheR or CheB

  Most likely, this balance would depend on the concentration of the attractant, which in this simple consideration only took on two extreme values.
- Particularly in biological systems, such fine tuning would be a challenge. The concentrations of CheR and CheB are relatively small; they are therefore likely to fluctuate quite strongly. For that reason this model is not very convincing, if the observed adaptation is as precise as it is observed in bacterial chemotaxis .

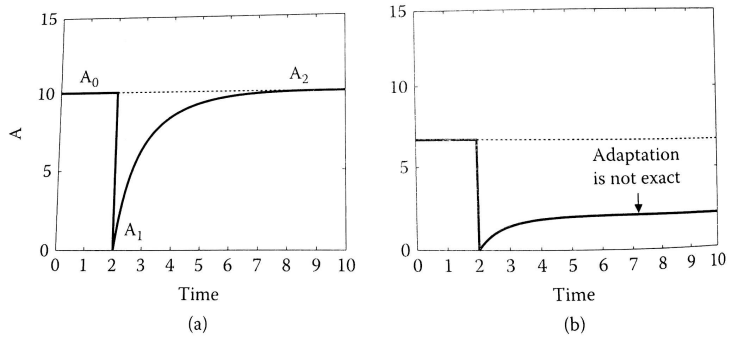

Figure 22: Sensitivity of the adaptation to the tuning of the parameters in (11). a) Perfectly tuned. b) When the CheR-level R is reduced by 20% perfect adaptation is missed by a factor of 3 (Alon, 2007).

Consider instead the reaction scheme of Fig.23.

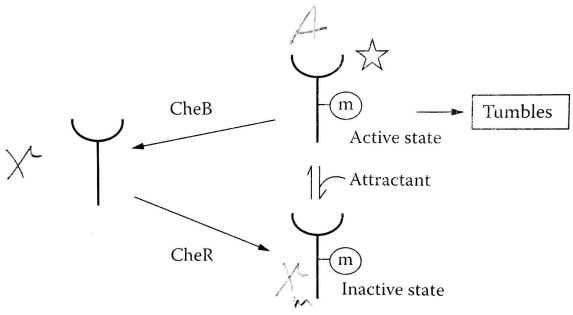

Figure 23: Reaction scheme of a minimal version of the Barkai-Leibler model for robust adaptation (Barkai and Leibler, 1997) as discussed in (Alon, 2007).

Only three states arise in this model

- inactive, unmethylated state X
- inactive, methylated state X_m
- active, methylated state X_m^*. Since this is the only active state denote it by A.

Key elements

- The attractant can bind to the active and the inactive methylated states.
- The attractant shifts the balance between the two methylated states: with attractant the reaction is more biased towards the inactive state.
- CheB demethylates only the active, but not the inactive state.

The methylation by CheR is again saturated, as in the fine-tuned adaptation model.

Consider the following, simplified model

$$\begin{aligned} \frac{dX}{dt} &= -V_R R \frac{X}{X+K_X} + V_B B\, A \\ \frac{dX_m}{dt} &= V_R R \frac{X}{X+K_X} - k(L)\, X_m + k'(L)\, A \\ \frac{dA}{dt} &= k(L)\, X_m - V_B B\, A - k'(L)\, A \end{aligned}$$

Note:

- In general, the demethylation by CheB should be taken to be nonlinear (Michaelis-Menten). The linearization is not necessary for the adaptation, but makes it easier to analyze.
- The methylation by CheR is written as Michaelis-Menten reaction, although it is known to be saturated. It would therefore be appropriate to consider the limit $K_X \to 0$. But to get insight into the mechanism it is useful to keep K_X, but take it to be small. The point is that the perfect adaptation *requires* the saturation.

Assuming $K_X \ll X$ we can expand

$$\frac{dX_m}{dt} = V_R R \frac{1}{1+\frac{K_X}{X}} - kX_m + k'A \approx V_R R - kX_m + k'A - K_X \frac{V_R R}{X} + \mathcal{O}(K_X^2)$$

Because the total receptor number is fixed, the equation for X need not be considered. Instead write

$$X = X_t - X_m - A$$

It turns out to be useful to write equations in terms of A and $X_{mt} \equiv X_m + A$, the total amount of methylated receptor,

$$\begin{aligned} \frac{dX_{mt}}{dt} &= V_R R - kX_m + k'A - K_X \frac{V_R R}{X} + kX_m - V_B B - k'A \\ &= V_R R - V_B B\, A - K_X \frac{V_R R}{X_t - X_{mt}} + \mathcal{O}(K_X^2) \end{aligned} \tag{12}$$

$$\frac{dA}{dt} = kX_{mt} - (V_B B + k + k')\, A \tag{13}$$

For the adaptation we are interested in the steady states.

For the completely saturated case $K_X = 0$ one gets

$$\begin{aligned} \frac{dX_{mt}}{dt} &= V_R R - V_B B\, A \\ \frac{dA}{dt} &= kX_{mt} - (V_B B + k + k')\, A \end{aligned}$$

yielding the fixed point

$$A = \frac{V_R\, R}{V_B\, B} \qquad X_{mt,0} = \frac{V_B B + k + k'}{k} \frac{V_R R}{V_B B}$$

Note:

- At this leading order
  - the activity A is determined by the differential equation for X_{mt} not that for A.
  - the activity A does not depend on the binding rates k and k', which depend on the concentration of the attractant $\Rightarrow$ the steady-state activity does not depend on the attractant concentration in this limit, the adaptation is perfect.
  - the steady-state activity does depend on the concentration of CheR and CheB and can therefore vary across bacteria.
  - the concentration X_m of the inactive methylated state *does* depend on the attractant concentration.
  - the time scale for the relaxation to the steady state does depend on parameters.

To assess what happens when methylation is not completeley saturated, expand A in K_X

$$A = A_0 + K_X A_1 \qquad X_{mt} = X_{mt,0} + K_X X_{mt,1}.$$

At $\mathcal{O}(K_X^0)$ we recover the result above

$\mathcal{O}(K_X)$:

$$-V_B B A_1 - \frac{V_R R}{X_t - X_{mt,0}} = 0 \qquad A_1 = \frac{1}{V_B B}\frac{V_R R}{X_t - X_{mt,0}}$$

Notes:

- Since $X_{mt,0}$ depends on the ligand concentration, the steady-state activity changes with the attractant concentration when saturation is not complete: adaptation becomes imperfect.

Revisit (12,13) to leading order,

$$\begin{aligned} \frac{dX_{mt}}{dt} &= a\,(A_{st} - A) \\ \frac{dA}{dt} &= kX_{mt} - bA \end{aligned}$$

The dynamics of X_{mt} determines the steady-state value of A: at the fixed point $A = A_{st}$ independent of all other parameters in the system. X_{mt} provides an *integral feedback control*: it integrates up the deviation of A from the target value

$$X_{mt} = a \int^t (A_{st} - A(t'))\; dt'$$

Thus

- As long as A has not reached the target value, X_{mt} grows and provides ever stronger feedback to A.
- The fixed point obtained by the control is stable for all positive values of a, k, and b. The Jacobian is given by
$$\mathbf{L} = \begin{pmatrix} 0 & -a \\ k & -b \end{pmatrix}$$
with $tr\mathbf{L} < 0$ ($\Rightarrow$ no Hopf bifurcation) and $det\mathbf{L} > 0$ (no steady bifurcation).
- Since the equation for X_{mt} does not depend on X_{mt} there is no scale for X_{mt}. Therefore X_{mt} can take on any value and can provide arbitrarily large drive to A.
Once the differential equation for X_{mt} does depend also on X_{mt}, as is the case if the saturation of CheR is not perfect, there is a characteristic value for X_{mt} and its ability

to integrate the error signal and with it its ability to shift A towards A_{st} is limited. E.g. look at evolution of X_{mt} (12) for small X_{mt}

$$\begin{aligned}\frac{dX_{mt}}{dt} &= V_R R - V_B B\, A - K_X \frac{V_R R}{X_t - X_{mt}} + \mathcal{O}(K_X^2) \\ &= V_R R - V_B B\, A - K_X \frac{V_R R}{X_t} - K_X \frac{V_R R}{X_t}\frac{X_{mt}}{X_t} + \mathcal{O}(X_{mt}^2, K_X^2)\end{aligned}$$

Thus, there is a term that pushes X_{mt} towards 0, limiting its ability to drive A.

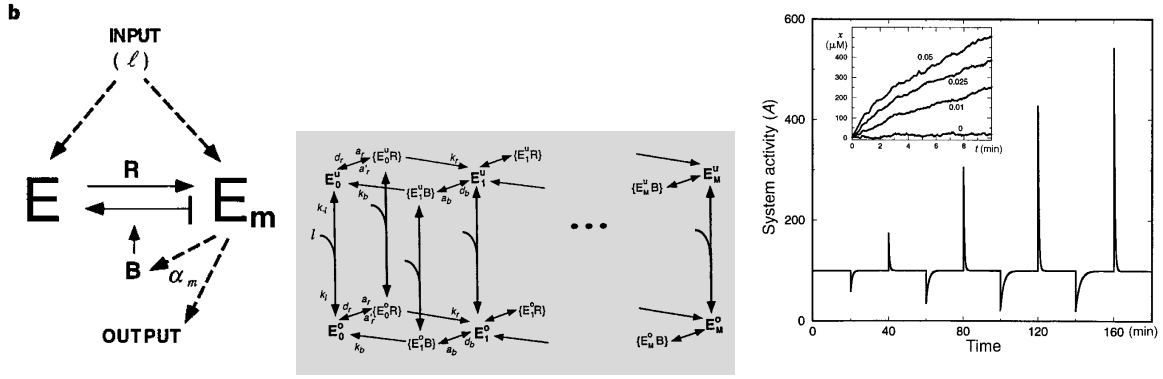

Figure 24: Barkai-Leibler model. Sketch of the minimal scheme and of the scheme involving multiple methylation levels. The methylation of E goes via the complex ER, whereas the demethylation goes via the complex EB. Time course of adaptation after addition and removal of increasingly larger ligand concentrations (Barkai and Leibler, 1997).

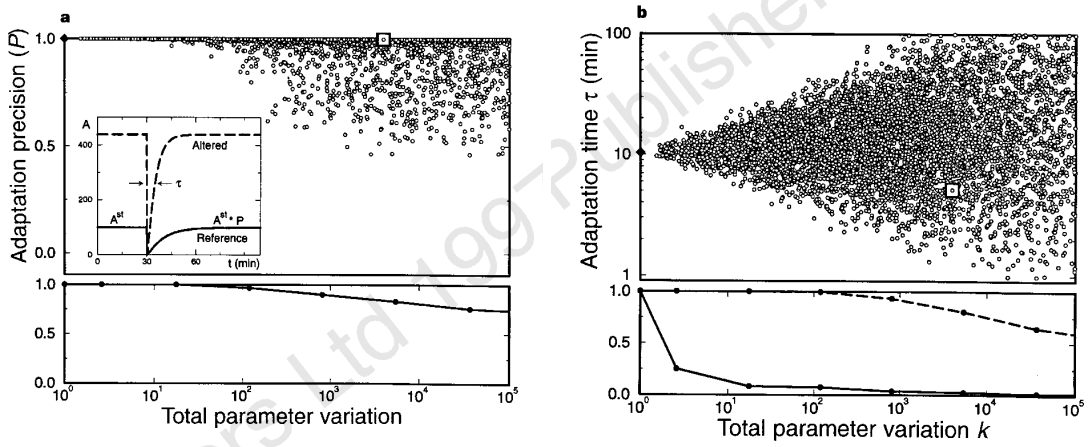

Figure 25: Robust adaptation in Barkai-Leibler model. The adaptation precision depends only weakly on the parameters of the problem, as characterized by the total parameter variation $\log k = \sum_n \left|\log\left(\frac{k_n}{k_n^0}\right)\right|$, where k_n is the modified value of the parameter compared to the reference value k_n^0 for which the adaptation is perfect. In contrast, the time scale of the adaptation depends strongly on the parameters (Barkai and Leibler, 1997).

1.5.1 Integral Feedback Control As a Dynamical System[11]

Consider a general dynamical system driven by some time-dependent input X with output Z and internal variable Y

$$\begin{aligned} \frac{dY}{dt} &= \epsilon F(X,Y,Z) \\ \frac{dZ}{dt} &= G(X,Y,Z). \end{aligned}$$

Our goal is

- strong, fast *transient* response in Z when X is changed
- *no long-term* response for whatever value of X.

Thus, there are two time scales that are relevant here

- Z responds quickly to reach some peak value $Z_p(X+\Delta X, X)$ when X is changed from X to $X+\Delta X$.
- Y responds slowly ($\epsilon \ll 1$) to adapt the system to the new input value of X, where then $Y = Y_s(X)$ and $Z = Z_s(X)$.

Quantification of our goal:

High sensitivity

$$S = \frac{|Z_p(X+\Delta X, X) - Z_s(X)|}{|\Delta X|} \qquad \text{large}$$

Small adaptation error

$$E = \frac{|Z_s(X+\Delta X) - Z_s(X)|}{|Z_p(X+\Delta X, X) - Z_s(X)|} \ll 1$$

[11] (Tu and Rappel, 2018)

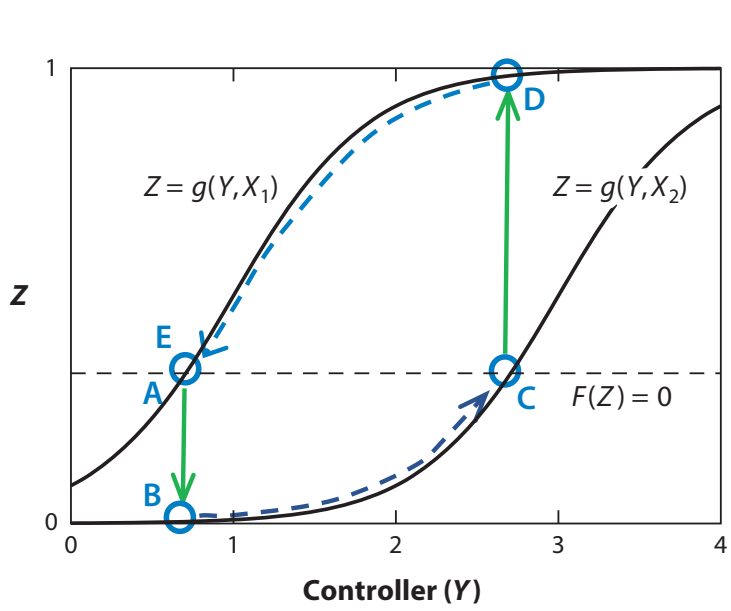

Figure 26: Phase plane with nullclines g(X,Y) according to (18) and $f(X,Z)$ chosen for perfect adaptation (Tu and Rappel, 2018).

As is typical for fast-slow systems, it is useful to consider the nullclines of the system

$$Z = g(X,Y) \qquad Y = f(X,Z).$$

For small changes $|\Delta X|$ and separated time scales on which Z and Y evolve we have

- the system starts at the intersection of the two nullclines, $(Y_s(X), Z_s(X))$ (point A in Fig.26.
- after a small change $X_1 \to X_2 = X_1 + \Delta X$ the system quickly approaches the nullcline of Z that is shifted due to the change in X, but with Y is still close to the previous value (B) since $\epsilon \ll 1$,

$$Z_p(X+\Delta X, X) \approx g(X+\Delta X, Y_s(x)) \approx \underbrace{g(X,Y_s(x))}_{Z_s(X)} + \Delta X \frac{\partial g(X,Y_s(X))}{\partial X}$$

- the adapted response is reached after Y evolves to its steady-state value[12],

$$\begin{aligned} Z_s(X+\Delta X) &= g(X+\Delta X, Y_s(X+\Delta X)) \\ &\approx \underbrace{g(X,Y_s(X))}_{Z_s(X)} + \Delta X \left(\frac{\partial g}{\partial X} + \frac{\partial g}{\partial Y}\frac{\partial Y_s}{\partial X} \right) \end{aligned}$$

[12]The derivatives are to be evaluated at X and $Y_s(X)$.

Thus,

$$E \approx \left| \frac{\frac{\partial g}{\partial X} + \frac{\partial g}{\partial Y}\frac{dY_s}{dX}}{\frac{\partial g}{\partial X}} \right| = \left| \frac{\partial g}{\partial X} \right| \left| 1 + \frac{\frac{\partial g}{\partial Y}\frac{dY_s}{dX}}{\frac{\partial g}{\partial X}} \right|.$$

Therefore, to have a small adaptation error a necessary condition is

$$\frac{\partial g}{\partial X} \cdot \frac{\partial g}{\partial Y}\frac{\partial Y_s}{\partial X} < 0 \tag{14}$$

i.e. the direct change of Z due to the change in X needs to be compensated by an opposite indirect change of Z via Y; the two pathways need to have opposite signs.

Look for a minimal system, i.e. with a minimal number of non-zero interactions.
To have a non-zero peak response we need

$$\frac{\partial g}{\partial X} \neq 0.$$

In order to be able to adapt at all we need

$$\frac{\partial g}{\partial Y} \neq 0.$$

Consider the case[13] $\frac{\partial g}{\partial X} < 0$, $\frac{\partial g}{\partial Y} > 0$.

We have

$$\frac{dY_s}{dX} = \frac{\partial f}{\partial X} + \frac{\partial f}{\partial Z} \underbrace{\frac{\partial Z_s}{\partial X}}_{\frac{\partial g}{\partial X} + \frac{\partial g}{\partial Y}\frac{\partial Y_s}{\partial X}}$$

Then we need

$$\frac{\partial Y_s}{\partial X} = \frac{\frac{\partial f}{\partial X} + \frac{\partial f}{\partial Z}\frac{\partial g}{\partial X}}{1 - \frac{\partial f}{\partial Z}\frac{\partial g}{\partial Y}} > 0 \tag{15}$$

Then, (15) can be satisfied with

1. Incoherent feed-forward loop
   Y and Z respond oppositely to X

   $$\frac{\partial f}{\partial X} > 0 \qquad \frac{\partial f}{\partial Z} = 0 \tag{16}$$

   in which case the second term in the denominator in (15) vanishes.

2. Negative feed-back loop
   Y is only driven (negatively) by Z

   $$\frac{\partial f}{\partial X} = 0 \qquad \frac{\partial f}{\partial Z} < 0 \tag{17}$$

   in which case the denominator is positive.

[13] The case $\frac{\partial g}{\partial X} < 0$, $\frac{\partial g}{\partial Y} > 0$ works analogously.

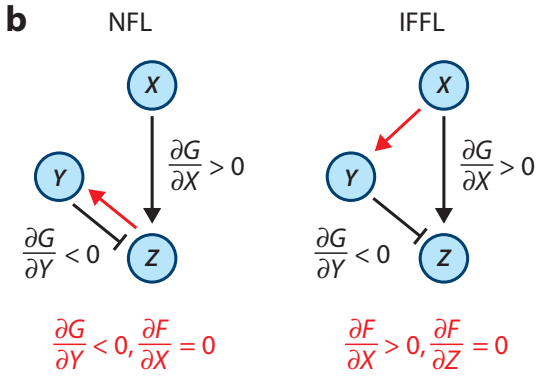

Figure 27: Sketch of the two minimal networks to achieve adaptation (Tu and Rappel, 2018).

Compare with the simple model (12,13) discussed before for perfect saturation: $A \to Z$, $X_{mt} \to Y$,

$$\begin{aligned} G(X,Y,Z) &= kY - (V_B + k(X) + k'(X))\, Z \\ \epsilon\, F(X,Y,Z) &= V_R R - V_B B\, Z, \end{aligned}$$

which matches case (17) of the negative feed-back loop. Since methylation and demethylation are much slower than ligand binding, i.e. $V_R R$ and $V_B B$ are small of $\mathcal{O}(\epsilon)$.

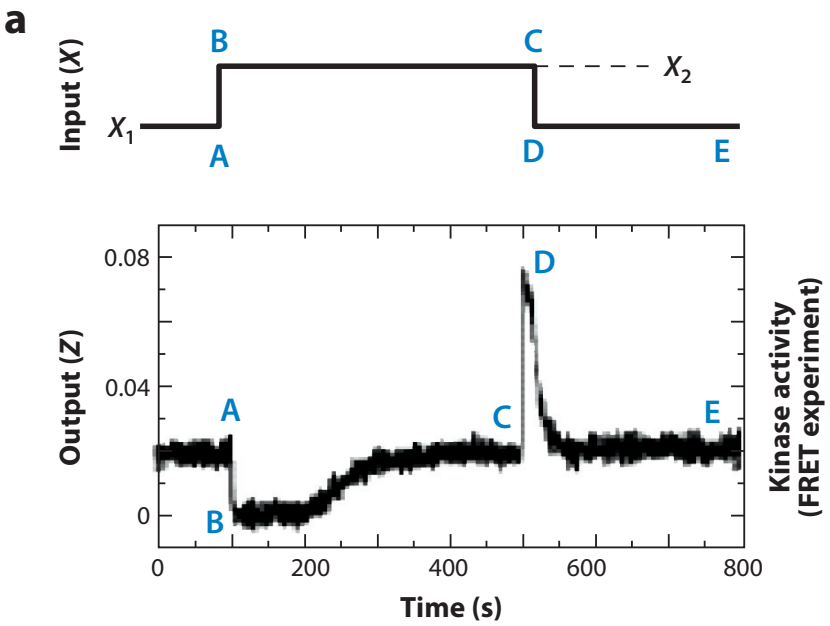

Figure 28: Experimentally observed adaptation of the response Z (kinase activity) to step changes in concentration in attractant. (Sourjik and Berg, 2002) as shown in (Tu and Rappel, 2018).

Experimentally, it has been found that the input-output relationship follows a sigmoidal form with a very large Hill coefficient. Part of this high sensitivity has been attributed to cooperativity between the different chemoreceptors, which are clustered near the pole of E. coli and other bacteria. Modeling this cooperativity yields for G the form

$$G(X,Y,Z) = -\frac{1}{\tau_Z} Z + \frac{1}{\tau_Z} \left(1 + e^{N f_m(Y)} \left(\frac{1+\frac{X}{K_i}}{1+\frac{X}{K_a}} \right)^N \right)^{-1} . \tag{18}$$

At this point we will not go into details of the modeling of the receptor cluster and just look at the results they obtained for the adaptation (e.g. (Mello et al., 2004)).

Increasing the concentration of the attractant shifts the Z-nullcline to larger values of Y. After an increase in concentration the output Z drops quickly to the new nullcline of Z. Then the system follows that nullcline during the adaptation process. It comes to an end at the new fixed point (Fig.26),

- Since $F = F(Z)$ is independent of Y and X that new fixed point has to have the same output as the previous fixed point.
- Any dependence of F on X or Y would generically destroy the perfect adaptation, unless it was explicitly *tuned* to keep the intersection of the nullclines at the same value of Z.

This model gives also good agreement for the response to sinusoidally varying attract concentrations. It shows that for low frequencies the adaptation mechanism essentially computes the time derivative of the concentration (Fig.29)

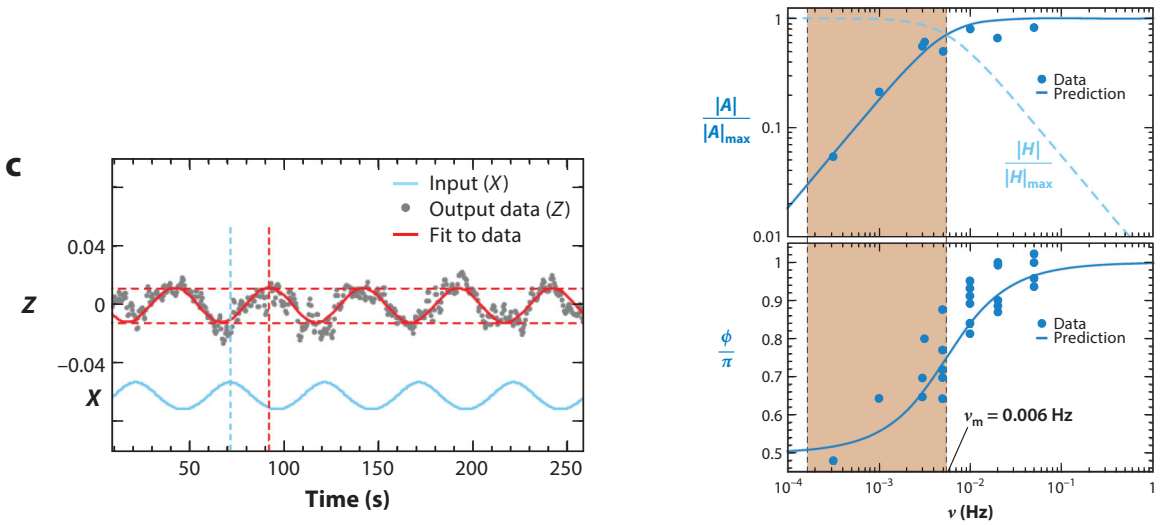

Figure 29: Adaptation response to sinusoidally varying concentrations (Tu and Rappel, 2018).

2 Morphogenesis

How do multicellular organisms develop? How do cells know when to differentiate and how and where they need to go? In simple animals many body parts can be regenerated and parts of the body can be grafted onto other bodies. An excellent example is hydra. Important work demonstrating that grafting the hypostome of one hydra onto another one can induce a second axis (e.g. #42 in Fig.31) was done by Ethel Browne in her PhD thesis Browne (1909). This was already well before Spemann and Mangold identified the organizers in salamander embryos (see below).

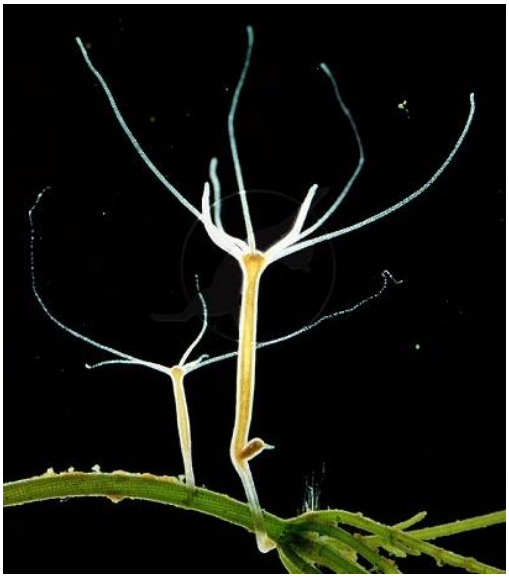

Figure 30: Hydra.

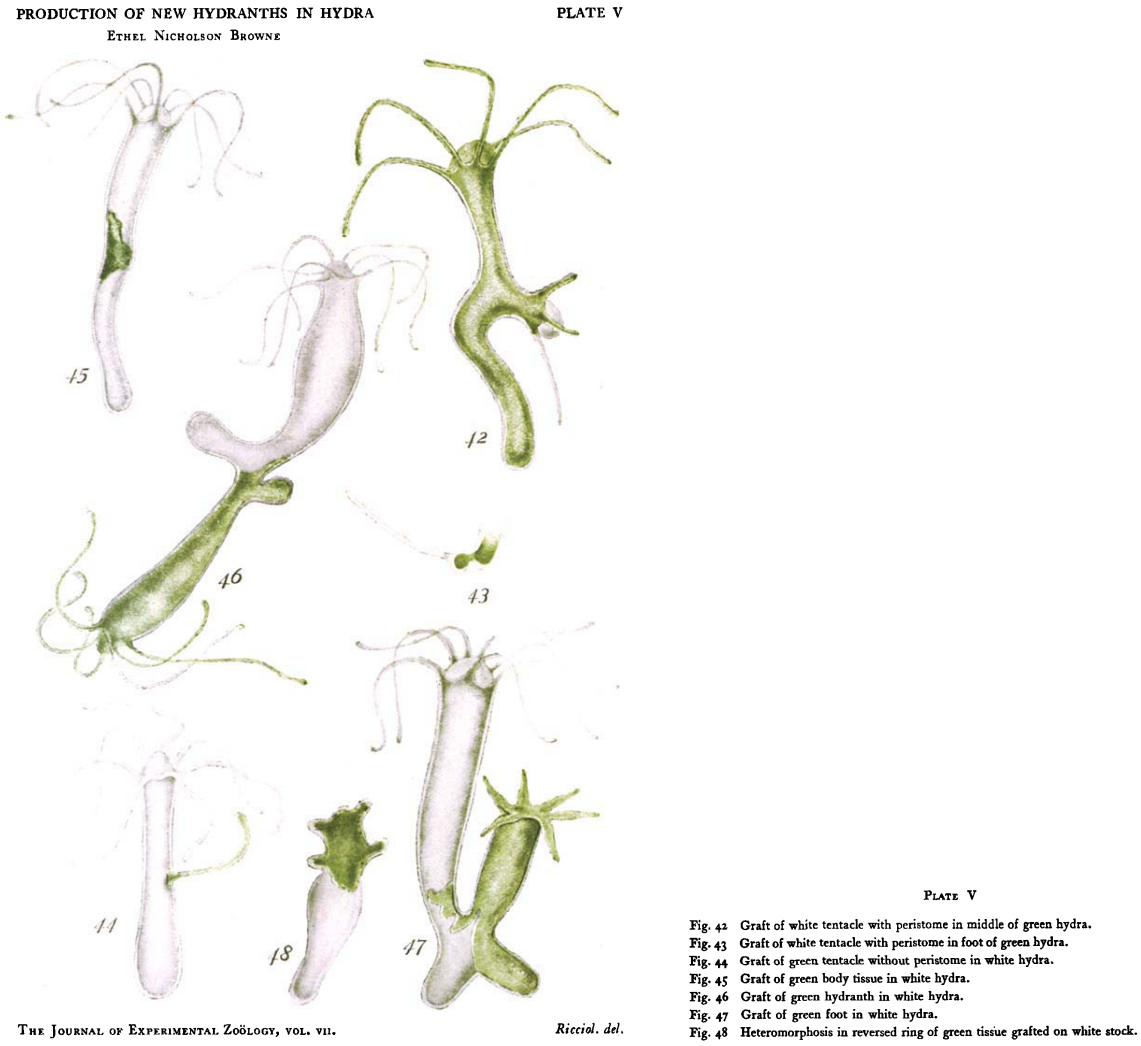

Figure 31: Hydra grafting. 42: graft of white tentacle makes whole additional hydranth, which involves also material from the green hydra: the cells from the white hydra seem to instruct the cells of the green hydra what to do. 47: graft of green foot on white hydra at foot end $\rightarrow$ full green hydra. (Browne, 1909)

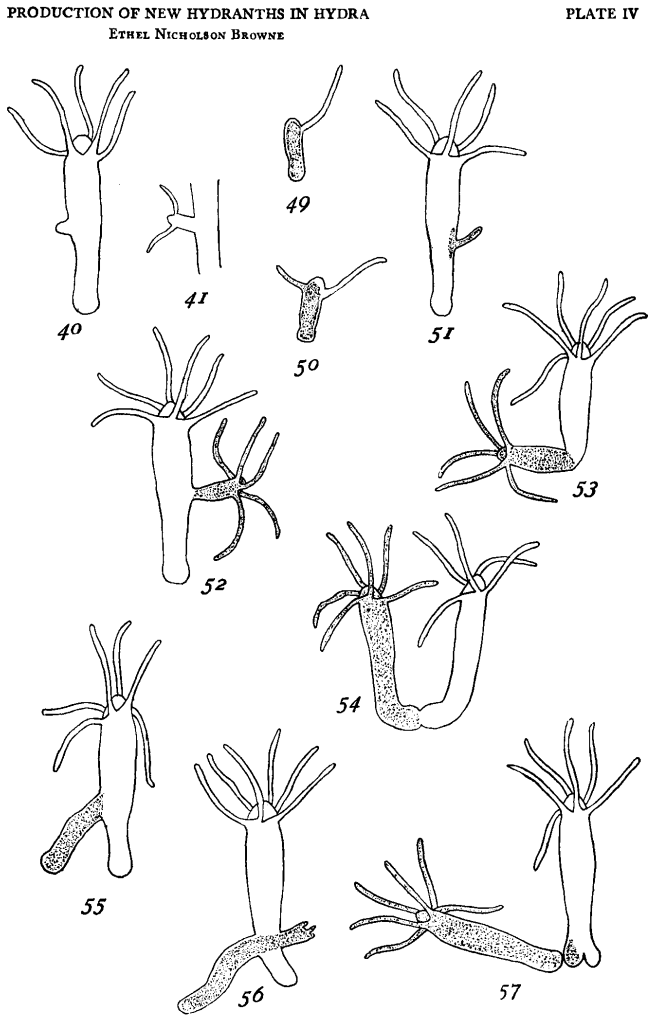

PLATE IV

Figs. 40–41. Graft of regenerating tissue.
Figs. 49–50 Small hydra produced by graft of white tentacle in foot of green hydra.
Fig. 51 Graft of green tentacle without peristome in white hydra.
Fig. 52 Graft of green hydranth in white hydra.
Figs. 53–54 Graft of green and white heads.
Figs. 55–57 Graft of green foot in white hydra.

Figure 32: Hydra grafting. 55-57: depending on the location of the graft, grafting foot onto foot may lead to another foot or a complete hydranth. (Browne, 1909)

What controls how a grafted body part will evolve?

Organizers: Spemann and Mangold (Spemann and Mangold, 1924) looked at the very early embryogenesis in salamander (Triton cristatus and Triton taeniatus), around the time of gastrulation. At that point the zygote has undergone many cell divisions but the cells are still quite undifferentiated, i.e. there are only two types of cells in two layers. At that stage one can transplant small pieces of tissue from one embryo to another, even between

different species:

- In most cases, the transplanted piece of tissue evolves like the tissue at the location to which it was transplanted. Thus, tissue that is taken from an area that would develop into brain tissue develops into epidermal tissue if it was transplanted to a location where the tissue develops into epidermal tissue. The tissue effectively adapts to its environment.
- However, tissue from a specific area behaves differently: it does not adapt; instead it determines the development of the surrounding tissue and generates an additional, secondary neural tube and can eventually lead to the development of a second head. This *organizer* tissue therefore determines the development of the surrounding tissue. The tissue of the secondary neural tube and organs involves also tissue from the host and not only from transplant itself.

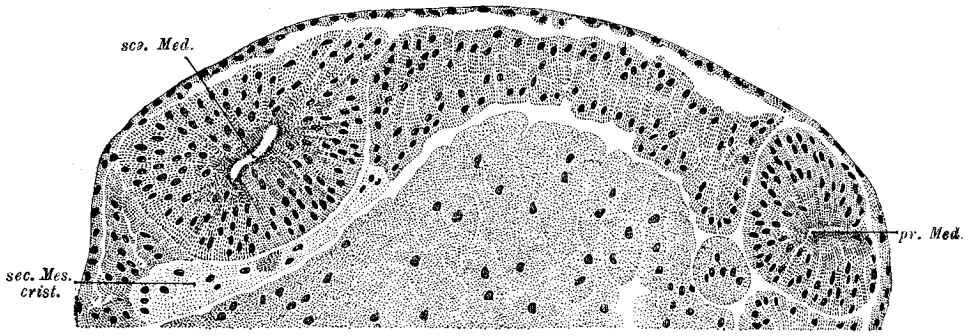

Fig. 4. Um 8b. *Cross section through the anterior third of the embryo (cf. Figs. 2 and 3) pr. Med., primary neural tube; sec. Med., secondary neural tube. The implant (light) is in the mesoderm (sec. Mes. crist.). 100X.*

Figure 33: Transplantation of tissue from one salamander embryo to another. The implant has lighter color; that was one of the important steps forward compared to earlier experiments of Spemann's. This allowed to establish that the second neural tube etc. were not made only of implanted tissue, but that the organizer recruited the host tissue as well. (Spemann and Mangold, 1924).

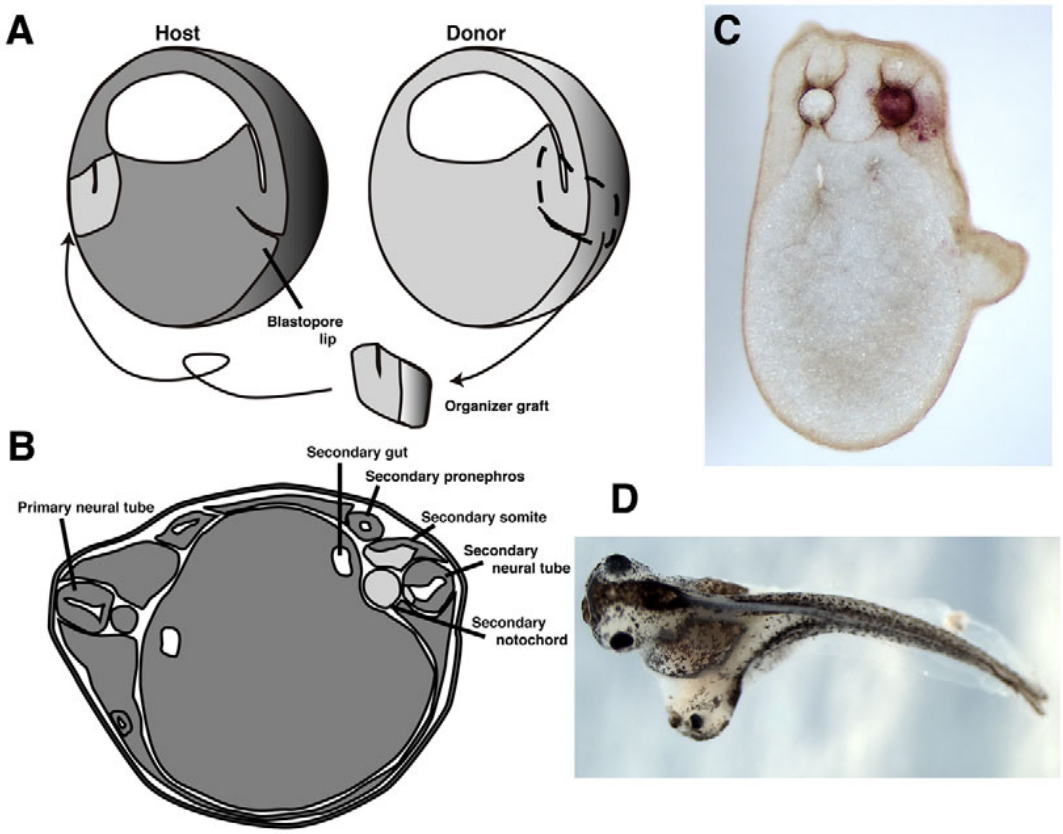

Figure 34: Implantation of a second organizer can lead to the development of a second head (Harland, 2008).

How is the information communicated from the organizer to the remaining tissue? It could be a chemical signal, a morphogen, or multiple morphogens (Turing, 1952). In the hydra, e.g., it could determine what becomes the head and what the foot.

2.1 Turing Model for the Formation of Periodic Structures

In 1952 Turing suggested that the combined activity of two (possibly more) morphogens, an activator and an inhibitor, could set up spatially periodic concentration profiles that could drive the formation of periodic structures. He mentioned as a possible specific example the formation of the tentacles of hydra in that paper, which are sort of periodically spaced around the mouth.

The key element is that the differentiation of the cells occurs in a translationally invariant system, i.e. via *spontaneous symmetry breaking.* The model is therefore formulated as

$$\begin{aligned} \frac{\partial u}{\partial t} &= D_u \frac{\partial^2 u}{\partial x^2} + f(u,v) \\ \frac{\partial v}{\partial t} &= D_v \frac{\partial^2 v}{\partial x^2} + g(u,v) \end{aligned}$$

with f and g allowing a homogeneous base state (u_0, v_0),

$$f(u_0, v_0) = 0 \qquad g(u_0 v_0) = 0.$$

Linearization around this base state

$$u = u_0 + \epsilon u_1 \qquad v = v_0 + \epsilon v_1$$

yields

$$\begin{aligned} \frac{\partial u_1}{\partial t} &= D_u \frac{\partial^2 u_1}{\partial x^2} + a u_1 - b v_1 \\ \frac{\partial v_1}{\partial t} &= D_v \frac{\partial^2 v_1}{\partial x^2} + c u_1 - d v_1 \end{aligned}$$

and the linear stability with a Fourier ansatz in space

$$u_1 = U(t) e^{iqx} \qquad v_1 = V(t) e^{iqx}$$

gives

$$\begin{pmatrix} \frac{\partial U}{\partial t} \\ \frac{\partial V}{\partial t} \end{pmatrix} = \underbrace{\begin{pmatrix} -D_u q^2 + a & -b \\ c & -D_v q^2 - d \end{pmatrix}}_{\mathbf{L}} \begin{pmatrix} U \\ V \end{pmatrix}$$

and

$$det\mathbf{L} = \left(-D_u q^2 + a\right)\left(-D_v q^2 - d\right) + bc \qquad trace\mathbf{L} = -D_u q^2 + a - D_v q^2 - d$$

We are interested in the appearance of steady rather than temporally oscillatory patterns $\Rightarrow$ assume

$$a < d,$$

which makes the $trace\mathbf{L}$ negative for all wave numbers $\Rightarrow$ no Hopf bifurcation.

We have

$$det\mathbf{L} = D_u D_v q^4 + q^2 \left(D_u d - D_v a\right) + bc - ad.$$

As parameters are varied, the determinant $det\mathbf{L}$ can vanish first for $q = 0$ or for $q > 0$. We are interested in the case $q > 0 \Rightarrow$ we need

$$bc - ad > 0$$

$$D_u d - D_v a < 0$$

Together with the condition $a < d$ this implies

$$\frac{D_v}{D_u} > \frac{d}{a} > 1$$

More precisely, the instability occurs first at a q_c^2 for which at its minimum $det\mathbf{L} - 0$. This requires

$$\frac{d\,det\mathbf{L}}{dq^2} = 2D_uD_vq_c^2 + D_ud - D_va = 0 \qquad q_c^2 = \frac{D_va - D_ud}{2D_uD_v} > 0$$

$$\frac{(D_va - D_ud)^2}{4D_uD_v} - \frac{(D_va - D_ud)^2}{2D_uD_v} = -\frac{(D_va - D_ud)^2}{4D_uD_v} = ad - bc$$

$$(D_va - D_ud)^2 = 4D_uD_v\,(bc - ad)$$

The onset of the instability occurs then at

$$bc = \frac{(D_va + D_ud)^2}{4D_uD_v}.$$

The key elements of the Turing instability are

- the activator is (effectively) autocatalytic and activates also the inhibitor
- the inhibitor inhibits itself and the activator
- the inhibitor diffuses faster than the activator $\Rightarrow$
  - a local bump in the activator drives also a local bump in the inhibitor
  - the inhibitor bump is wider than the activator bump
  - the more localized activator bump sustains itself,
  - the activator bump is kept from spreading by the inhibitor bump
  - only at distances at which the inhibitor has sufficiently decayed the activator can arise again $\Rightarrow$ spatially periodic structure

With respect to hydra Meinhardt (earlier with Gierer) developed a more elaborate model comprised of 3 activator-inhibitor systems, one each for the head, for the foot, and for the tentacles. In addition, that model includes a long-range gradient in the source density for the generation of the activator that establishes and maintains the head-foot polarity Meinhardt (1993).

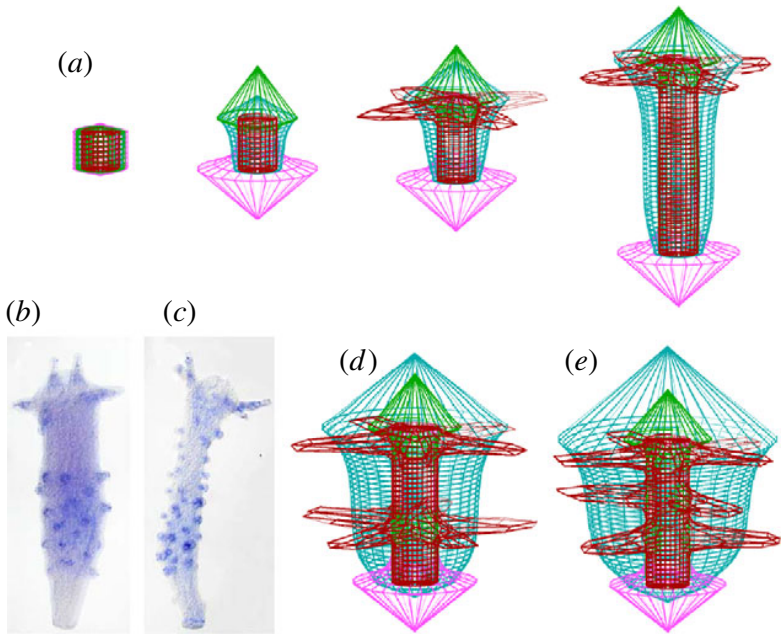

Figure 35: (a) Normal development of hydra within the Meinhardt model. (b,c) Exposure to the drug alsterpaullone leads to additional tentacles along the body of the hydra (*wnt* is strongly expressed at the tips of the tentacles). (d,e) This can be captured qualitatively in the model. (from Meinhardt (2012)).

Notes:

- It is not clear if/to what extent these molecular gradients have been confirmed experimentally.
- Diffusion is probably not the only communication between cells. Tentacle formation requires *notch*-signaling, which is based on cell contact. Notch receptors interact with transmembrane proteins of the adjacent cells and triggers regulation of gene expression in the nucleus.
- For smaller system sizes the long-range inhibition can stabilize polarization of the system rather than generate periodic structures.
- Inherent in the spontaneous symmetry breaking is that noise plays a significant role in establishing the patterned state, since the perfect unpatterned state exists below and above the threshold for the formation of the pattern. That raises the question whether in its original form it is robust enough to generate patterns for which precision and reliability is important (e.g. limb formation, in contrast to pigment patterns on fish skin, say).

2.2 Drosophila Development

The early development of drosophila embryos has been studied extensively and there is a wealth of information available by now. Consider it as an example.

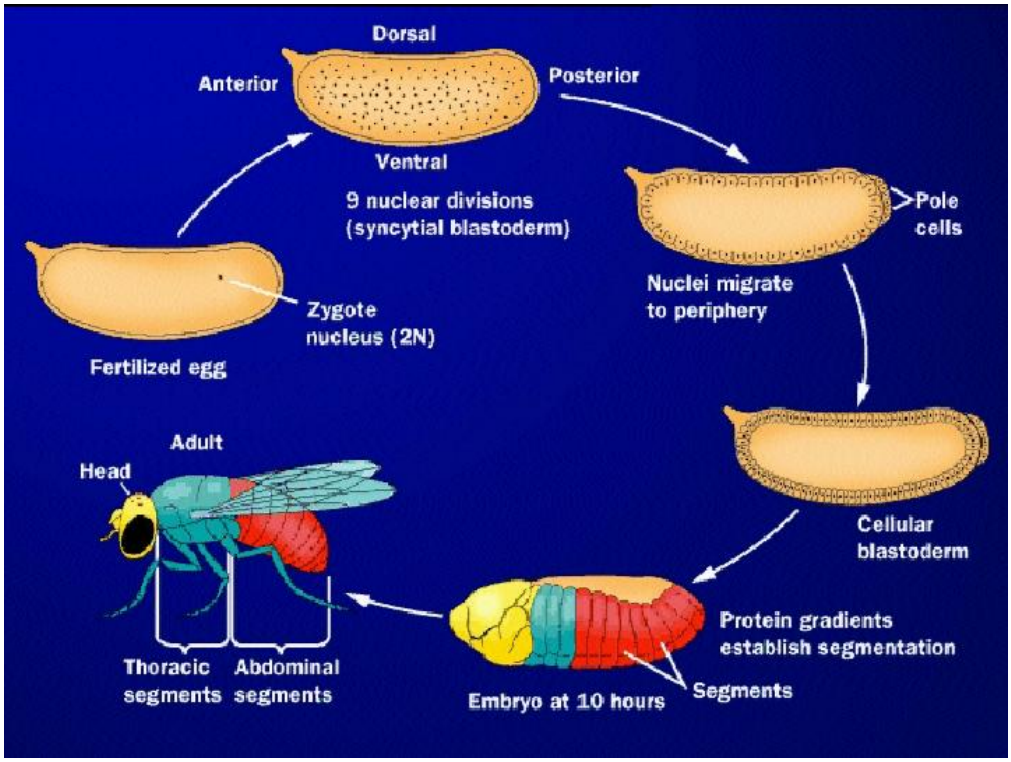

Figure 36: Life cycle of drosophila (from Purves et al. (1998)) .

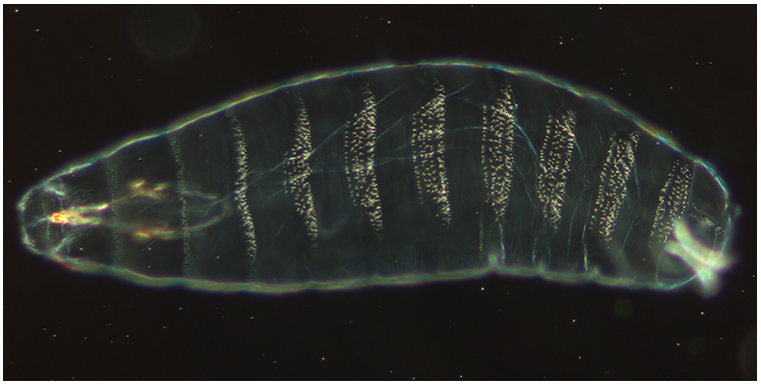

Figure 37: Drosophila: 22-hour-old embryo showing denticle bands on the cuticle. Head on the left (Wikipedia).

The main stages of early embryonic development of drosophila are[14]

- fertilization of the egg, making it a zygote

[14] 3 great videos by E. Wischaus are at https://www.ibiology.org/development-and-stem-cells/bicoid/ . see also https://www.ibiology.org/speakers/eric-wieschaus/

- 9 cycles of divisions of the nuclei generating 256 nuclei (each taking ~8 minutes). The zygote does not grow during that time and the nuclei are not separated by cell walls.
- During the 10th cycle the nuclei migrate to the periphery of the cell creating the syncytial blastoderm.
- After the 13th cycle (~4 hours after fertilization) cell walls form between the ~6,000 nuclei ('cellularization'), forming the cellular blastoderm.
  - At this point the cells have not differentiated yet, but the expression of various genes shows pre-patterns that direct the subsequent development and differentiation of the cells.
- Gastrulation
- ...

4 Hierarchies of Genes Involved in Morphogenesis

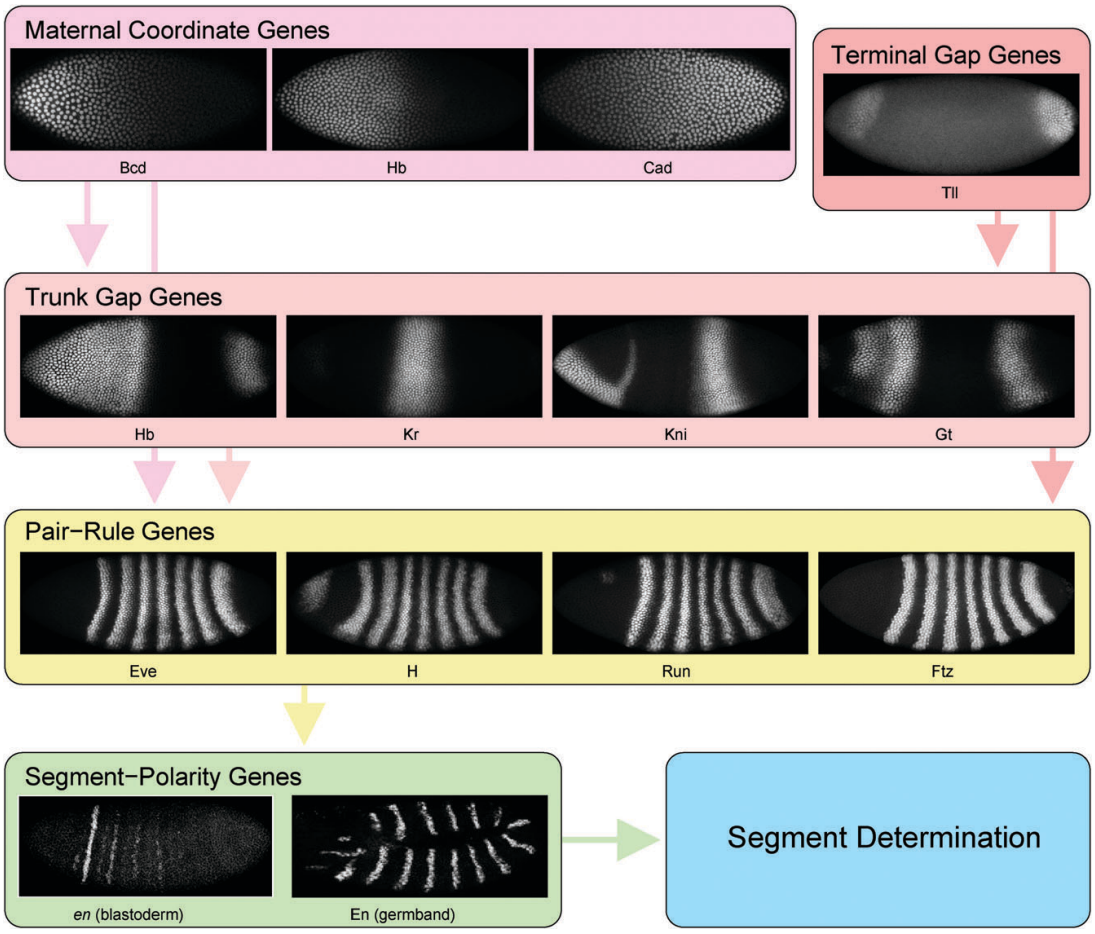

Figure 38: Hierarchy of maternal and zygotic genes (Jaeger, 2009).

Differentiation is controled by 4 generations of genes, which provide successively finer spatial control, with the genes operating on larger scales controling those operating on smaller scales

- maternal genes
  - *bicoid* (bcd), *hunchback* (hb), and *caudal (cad)*
    the mRNA for these proteins are deposited by the mother on the egg, giving the cell polarity:
    - *bcd* mRNA is expressed at the anterior end
    - *hb* and *cad* mRNA are expressed uniformly along the anterior-posterior axis
    - the translation of the corresponding proteins starts with the fertilization of the egg
- zygotic genes
  - gap genes
    - *hb* (zygotic *hunchback* transcription and translation enhances the protein translated from maternal mRNA)*, Krüppel* (*Kr*)*, knirps* (*kni*)*, giant* (*gt*)
  - pair-rule genes
    - *even-skipped* (*eve*) and others
  - segment-polarity genes

We focus here on the gradient of *bicoid*. *Bicoid* was the first protein to be recognized to be a morphogen (Driever and Nusslein-Volhard, 1988). It sets the stage for the further spatial organization.

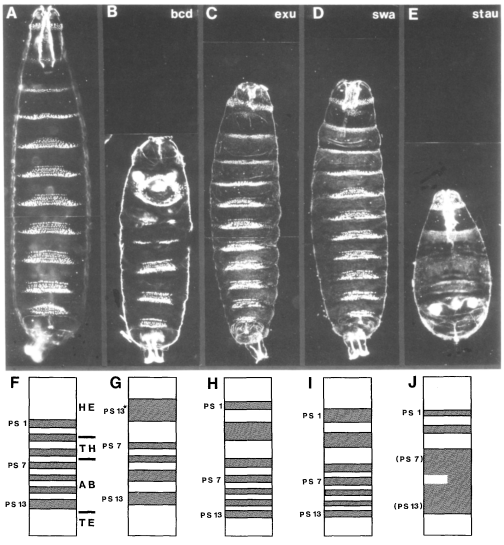

Figure 39: Maternal mutations that reduce expression of *bicoid* lead to substantially different embryos (bottom row give sketch of expression of *eve*. a) wildtype, b) Strong *bcd* mutant (almost no bcd), head and thorax replaced by a duplicated telson (sort of tail, marked $PS13^*$), c,d) Mutations with only moderately suppressed *bcd* (Driever and Nusslein-Volhard, 1988).

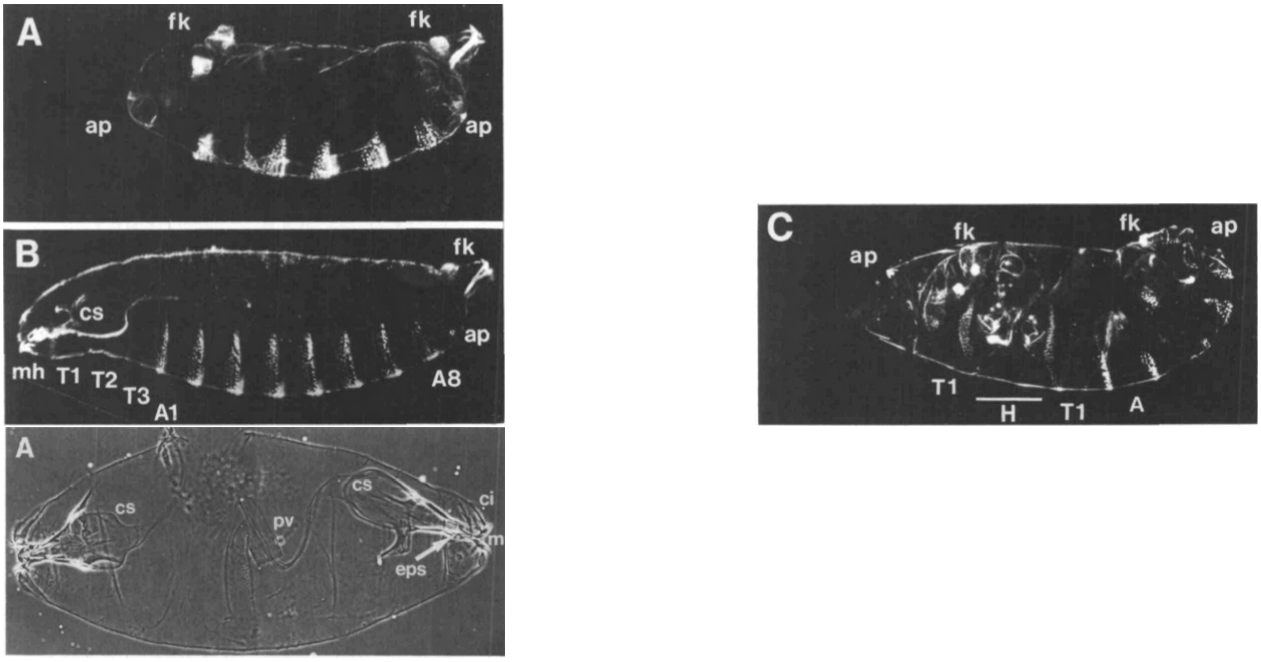

Figure 40: *bicoid* autonomously controls development: a) Severely impacted development of an embryo coming from mother with strong *bcd* mutation b) Injecting *bcd* mRNA rescues that development (cf. Fig.39b). c) Injection in the middle generates additional head (marked H). d) injection at the posterior end generates symmetric head formation (Driver et al., 1990).

2.3 The French Flag Model and Extensions

How could the morphogen direct the spatial differentiation? The concentration could provide *positional information* if a sufficiently large concentration gradient can be established. A very influential model along these lines was the french-flag model of Wolpert (Wolpert, 1969).

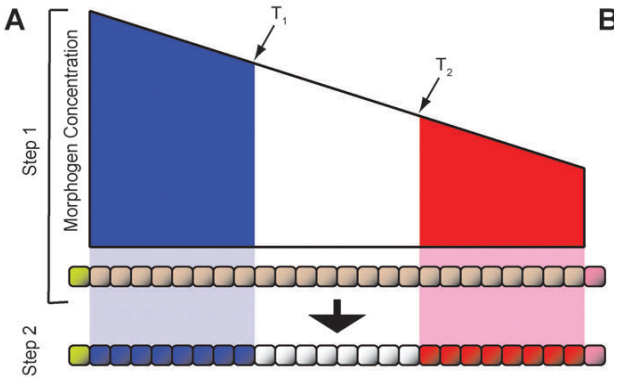

Figure 41: French flag model (Wolpert, 1969).

In a minimal version one could imagine that the concentration of the morphogen is fixed at the two ends of the organism. In the absence of any degradation its concentration is

then linear and the concentration defines a coordinate system. With suitable thresholds subsequent gene expression can be directed.

$$\frac{dm}{dt} = D\frac{d^2m}{dx^2} \qquad c(0) = c_0 \qquad c(L) = c_L$$

Question: is there enough time to set up such a (linear) gradient during development? Crick estimated the diffusion of the - at that time hypothetical - morphogen. He assumed a molecular weight of the order of 500 and a viscosity corresponding to that of a strong sucrose solution (40% by weight) (Crick, 1970) ,

$$D = \mathcal{O}(10^{-6}\frac{\mathsf{cm}}{\mathsf{s}^2})$$

He concluded that within 3 hours (10^4 s) a gradient of 700μm could be built up, which would correspond to roughly 70 cells. That size is of the order of the size that Wolpert discussed for various embryonic developments (not drosophila).

Back to drosophila: what is known about the concentration profile of bcd?

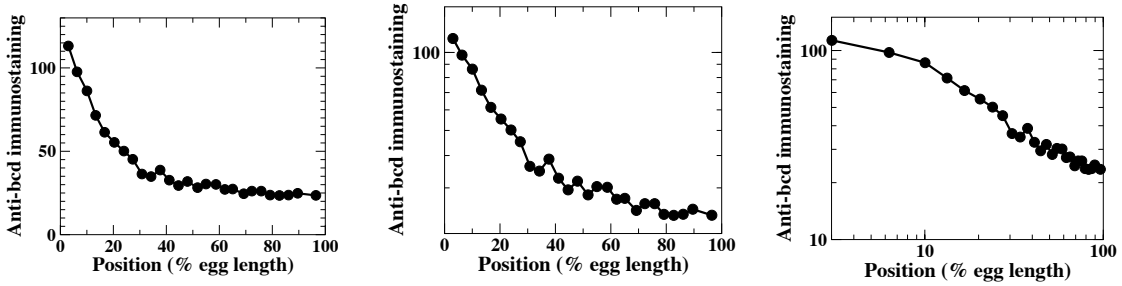

Figure 42: The same bcd-concentration in drosopila (from (Driever and Nusslein-Volhard, 1988)) plotted linearly (a), logarithmically in y (b), and double-logarithmically (c).

The concentration profile is clearly not linear

- the diffusion coefficient could be space-dependent $D(x)$ or depend on the morphogen concentration $D(m)$,
- the protein could become degraded with time

Model with fixed degradation rate

$$\frac{dm}{dt} = -\alpha m + D\frac{d^2m}{dx^2}$$

For *bcd* it is known that the protein is translated from the mRNA that is localized near the anterior end. Assume as boundary conditions

$$\left.\frac{dm}{dx}\right|_{x=0} = -J \qquad \left.\frac{dm}{dx}\right|_{x=L} = 0.$$

In steady state one obtains then an exponential profile

$$m(x) = m_0 e^{-\frac{x}{\lambda}} \qquad m_0 = \sqrt{\frac{D}{\alpha}} J \qquad \lambda = \sqrt{\frac{D}{\alpha}} \tag{19}$$

How robust does such a gradient define a location? The flux J depends on the mRNA concentration, which could well vary between cells. How much would this change the location. Assume the threshold m_θ for triggering subsequent differentiation is fixed

$$m_\theta = m(x_1; J_1) = \lambda J_1 e^{-\frac{x_1}{\lambda}} \overset{!}{=} m(x_2; J_2) = \lambda J_2 e^{-\frac{x_2}{\lambda}}$$

$$x_2 - x_1 = \lambda \ln \frac{J_1}{J_2} \qquad \Rightarrow x_2 - x_1 \sim 0.7\lambda \quad \text{for } J_2 = 2J_1$$

Since λ sets the scale over which the concentration gradient varies, the size of the various domains of the french flag cannot be much larger than λ otherwise the threshold m_θ separating the second from the third domain becomes too small to be reliably measured.

Therefore it has been suggested that an exponential decay does not allow robust patterning (Eldar et al., 2003). In a different context - the development of the drosophila wing, i.e. in the patterning of the morphogens Wg and Hh of the imaginal wing disc - they suggest that the profile should be steep near the source but shallow in the regions that define the domains. This would allow large variations of the source current without shifting the domain boundaries too much $\Rightarrow$ assume the degradation is nonlinear in the concentration

$$\frac{dm}{dt} = -\alpha m^2 + D\frac{d^2m}{dx^2}.$$

Consider again the steady state

$$D\frac{d^2m}{dx^2} = \alpha m^2$$

Try a power law

$$m(x) = Ax^p$$

$$Dp(p-1)\, Ax^{p-2} = \alpha\, A^2 x^{2p}$$

$$p - 1 = 2p \qquad \Rightarrow \qquad p = -2 \qquad \text{and} \quad A = \frac{6D}{\alpha}$$

$$m(x) = \frac{6D}{\alpha} x^{-2}$$

This solution diverges at $x = 0$:

- boundary condition needs to be placed somewhere else:

$$\left.\frac{dm}{dx}\right|_{x=b} = -J \quad \Rightarrow \quad -2\,\frac{6D}{\alpha} b^{-3} = -J \qquad b = \left(\frac{J}{2}\frac{\alpha}{6D}\right)^{-\frac{1}{3}}$$

  which implies

$$m(b) = \frac{6D}{\alpha}\left(\frac{J}{2}\frac{\alpha}{6D}\right)^{\frac{2}{3}} = \left(\frac{6D}{\alpha}\right)^{\frac{1}{3}}\left(\frac{J}{2}\right)^{\frac{2}{3}} \quad \text{or} \quad J = 2\left(\frac{\alpha}{6D}\right)^{\frac{1}{2}} m(b)^{\frac{3}{2}}$$

- even large variations in J can be accommodated with small shifts in the boundary position

$$\begin{aligned} b_2 - b_1 &= \left(\frac{J_2}{2}\frac{\alpha}{6D}\right)^{-\frac{1}{3}} - \left(\frac{J_1}{2}\frac{\alpha}{6D}\right)^{-\frac{1}{3}} \\ &= \left(\frac{J_1}{2}\frac{\alpha}{6D}\right)^{-\frac{1}{3}} \left(\delta^{-\frac{1}{3}} - 1\right) \qquad \text{for } \delta = \frac{J_2}{J_1}. \end{aligned}$$

Thus, for $J_1 \to \infty$ at fixed δ one has $b_2 - b_1 \to 0$, i.e. the change in the distance from the domain location at which $m = m_\theta$ becomes very small for large $J_{1,2}$. Specifically, with $m(x_\theta) = m_\theta$ we have

$$x_\theta = \sqrt{\frac{6D}{\alpha m_\theta}}$$

and

$$\begin{aligned} \frac{b_2 - b_1}{x_\theta} &= \left(\delta^{-\frac{1}{3}} - 1\right) \left(\frac{\alpha}{6D}\right)^{-\frac{1}{3}+\frac{1}{2}} \left(\frac{J_1}{2}\right)^{-\frac{1}{3}} m_\theta^{\frac{1}{2}} \\ &= \left(\delta^{-\frac{1}{3}} - 1\right) \left(\frac{\alpha}{6D}\right)^{-\frac{1}{3}+\frac{1}{2}-\frac{1}{6}} \left(\frac{m_\theta}{m(b_1)}\right)^{\frac{1}{2}} \\ &= \left(\delta^{-\frac{1}{3}} - 1\right) \left(\frac{m_\theta}{m(b_1)}\right)^{\frac{1}{2}} \end{aligned}$$

To get robustness, the concentration at the end of the system must be much larger than at the domain boundaries that are to be defined by the gradient: to get 10% accuracy one needs concentrations at the boundary that are a factor of 100 larger than inside the domain. Is that realistic?

Reassess the concentration profiles for *bicoid*:

- the concentration varies by a factor of 10 over the whole system
- for this mechanism to be operating one should see power-law behavior particularly for large concentrations. However, near the anterior end the behavior is nicely exponential and clearly not a power-law.

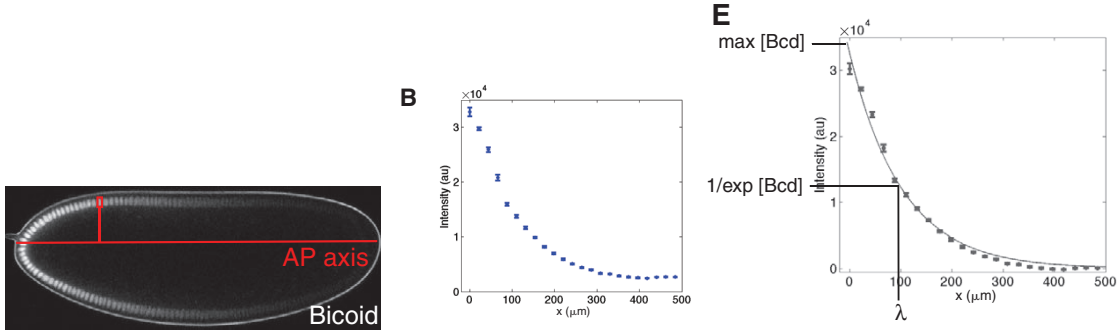

Figure 43: More recent measurements of $bicoid$ concentration using fluorescence (using venus, a GFP-derivative (Little et al., 2011)). There is a baseline level of fluorescence, which is subtracted when fitting to the exponential (Grimm et al., 2010).

Note:

- It is not clear that this type of robustness, while mathematically possible, is implemented in the *bicoid* system. Clearly, to answer questions like this good quantitative measurements as in Fig.43 are required.

Egg Sizes

Another dimension of robustness regards the size of the eggs

- Different species of drosophila differ significantly in their size, as do their eggs.
- The expression patterns scale with the egg size.

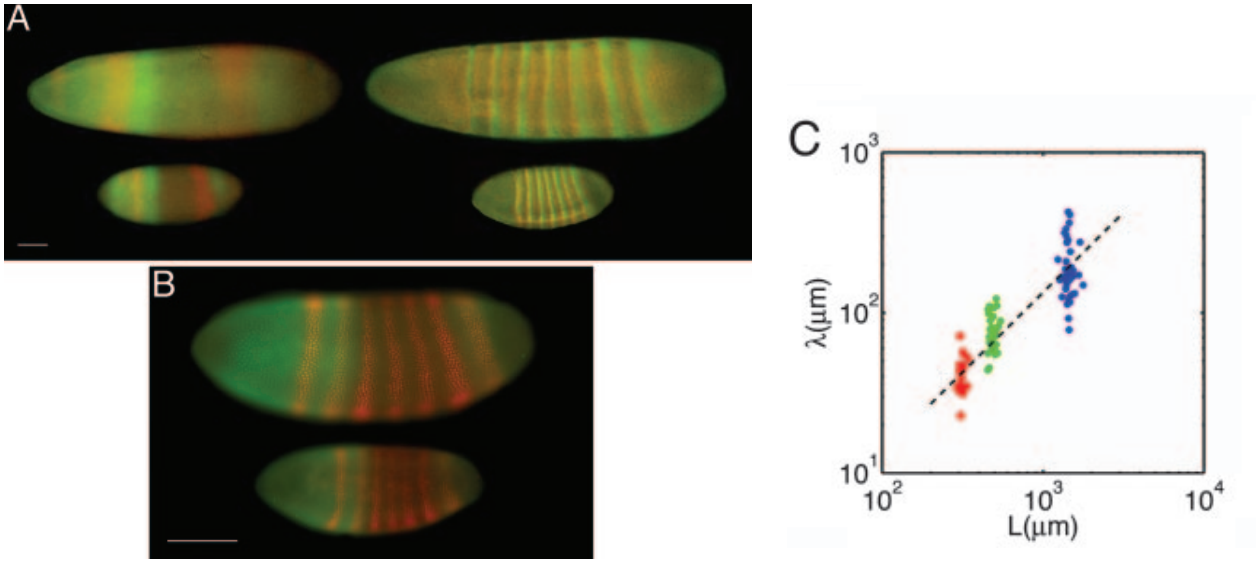

Figure 44: a) Embryos of L. sericata (upper) and D. melanogaster (lower) with *hunchback* (green) and giant (red). B) Embryos of D. melanogaster (upper) and D. susckii (lower) with *hunchback* (green) and *runt* (red). b) The length constants λ (cf. (19)) scale across species with the size of the embryos; however, within the species the length constants vary significantly (Gregor et al., 2005).

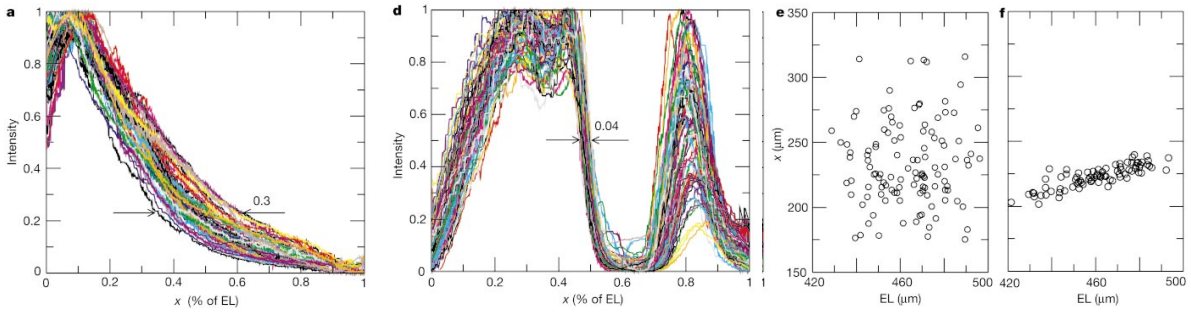

Figure 45: The location of the *bicoid* concentration boundary is much more variable than that of the *hunchback* concentration. (a,b) Concentration profiles. (c) In contrast to the *bicoid* position the *hunchback* position scales with the individual egg sizes (with the species) (Houchmandzadeh et al., 2002).

The *hunchback* gradient is much more precise than that of *bicoid*

- The standard deviation of the domain size as defined by *bcd* is 7% of the embryo size:, in 50% of the embryos the boundary is off by 5 nuclei.
- For *hb* the standard deviation is only 1% of the embryo size: it is precise to within a single nucleus

How does the *hunchback* gradient know about the embryo size, but the *bicoid* gradient does not?

- One possibility is that *hb* interacts with another gene that is localized posterior (Houchmandzadeh et al., 2005; McHale et al., 2006) $\Rightarrow$ homework problem.

3 Aggregation of Dictyostelium Discoideum

The slime mold Dictyostelium discoideum is an interesting organism. Much of its life it is a unicellular amoeba roaming for food, i.e. bacteria like E. coli. It finds its prey using chemotaxis detecting the folic acid that the bacteria secrete. When the food supply is depleted the amoeba start to aggregate and form a mound and then a slug. The slug consists of up to 10^5 cells. It moves towards light, heat, and humidity to find better conditions. Then the cells differentiate into stalk cells and spore cells and the slug transforms into a stalk with the spores on top. From there the spores are dispersed and become new amoebae (myxamoebae).

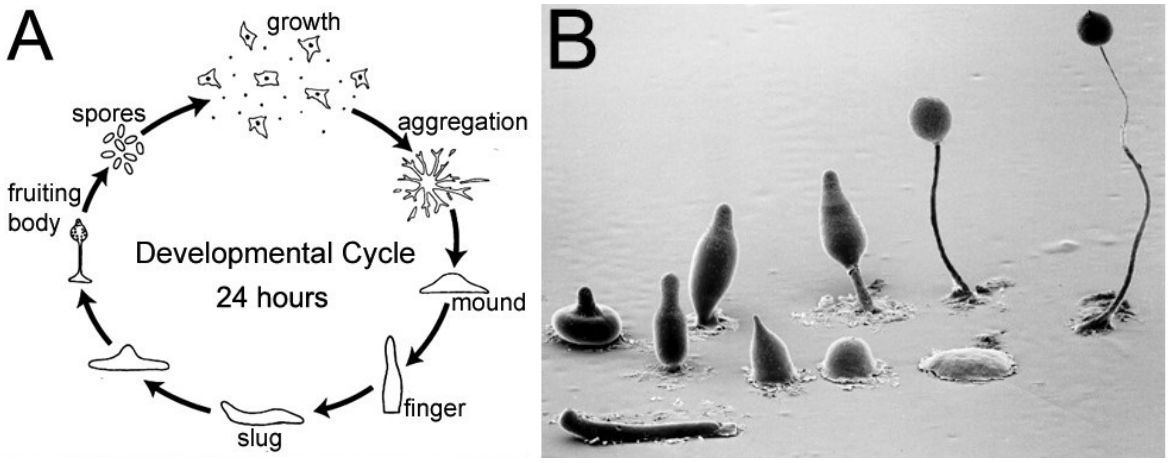

Figure 46: Life cycle of Dictyostelium discoideum.
(https://openi.nlm.nih.gov/detailedresult.php?img=PMC3352040_1423-0127-19-41-1&req=4)

The aggregation stage has attracted some interesting modeling efforts. The aggregation is based on two key features[15]

[15]Videos of Dictyostelium aggregating etc.:
https://www.youtube.com/watch?v=5h8WOWEqP6o
https://www.youtube.com/watch?v=tpdIvlSochk
https://www.youtube.com/watch?v=bkVhLJLG7ug

- Each amoeba acts as an excitable element (Noorbakhsh et al., 2015; Sgro et al., 2015): upon sensing a sufficient amount of cAMP it becomes excited and releases cAMP itself. After this excitation the amoeba becomes for some time unresponsive to further inputs. That is its refractory phase..
  The sensing and releasing of cAMP allows the amoebae to communicate with each other through cAMP waves that propagate across the population.
- Upon sensing cAMP each amoeba moves towards the perceived source of cAMP. This drives the aggregation of the amoeabe.

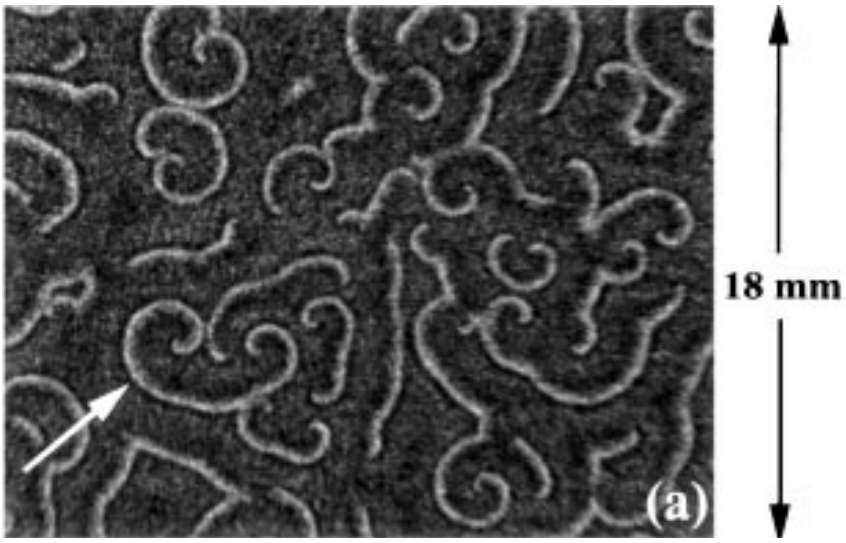

Figure 47: cAMP spiral waves during the aggregation of Dictyostelium discoideum (Goldstein, 1996).

Excitability

A standard minimal way to model an excitable system is using a two-component fast-slow system

$$\begin{aligned} \frac{dx}{dt} &= \frac{1}{\epsilon}F(x,y) \\ \frac{dy}{dt} &= G(x,y) \end{aligned}$$

with $\epsilon \ll 1$ and taking an N-shaped nullcline for x and a linear nullcline for y.

After infinitesimal perturbations away from the fixed point (intersection of the two nullclines) the trajectory returns immediately to the fixed point. After perturbations above a certain threshold the system makes a large excursion, which in this example reaches the left branch of the F-nullcline, which it then follows slowly to the local maximum at which the systems proceeds quickly to the branch of the nullcline. It then relaxes slowly back to the fixed point.

Excitable system have a (relative) refractory period after the excursions during which only extremely large (if any) perturbation can drive an excursion.

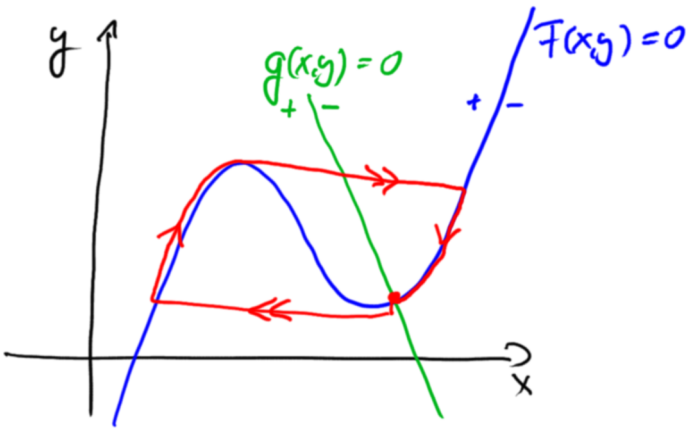

Figure 48: Nullclines and excursion from fixed point in standard excitable system.

Chemotaxis

Compared to our previous discussions of chemotaxis there are two important differences

- amoeabae are large enough ($\mathcal{O}(10\mu$m) to sense gradients by comparing concentration differences across there bodies, no run-tumble.
- the concentration gradients consist of propagating waves of cAMP rather than stationary gradients.

A minimal model for the chemotactic response of an amoeba at position x to a chemoattractant S traveling with wave speed v is therefore (Goldstein, 1996)

$$\frac{dx(t)}{dt} = r\frac{d}{dx}S(x(t) - vt).$$

It is useful to go into a moving frame $z = x - vt$ because it allows the separation of variables

$$\frac{dz}{dt} = r\frac{d}{dx}S(z) - v$$

$$\lambda\left\langle \frac{1}{rS'(z) - v}\right\rangle \equiv \int_{z_0}^{z_0+\lambda} \frac{dz}{rS'(z) - v} = \tau$$

where τ is the time the amoeba takes to cover one period λ of the wave. In the moving frame this amounts on average to a velocity

$$\bar{v}^{(z)} = \frac{\lambda}{\tau}.$$

Back in the stationary frame this yields then

$$\bar{v} = \frac{1}{\left\langle \frac{1}{rS'(z)-v}\right\rangle} + v.$$

Typically, the wave speed is much larger than the velocity of the amoeba. Therefore expand $\bar{v}$ in $1/v$

$$\frac{1}{rS'(z)-v} = -\frac{1}{v}\frac{1}{1-\frac{rS'}{v}} = -\frac{1}{v}\left(1+\frac{rS'}{v}+\left(\frac{rS'}{v}\right)^2+\dots\right)$$

and

$$\begin{aligned}\bar{v} &= -v\left(\frac{1}{\left\langle 1+\frac{rS'}{v}+\left(\frac{rS'}{v}\right)^2+\dots\right\rangle}-1\right)\\ &= v\left(\left\langle\frac{rS'}{v}\right\rangle+\left\langle\left(\frac{rS'}{v}\right)^2\right\rangle-\left\langle\frac{rS'}{v}\right\rangle^2+\mathcal{O}\left(\frac{1}{v^3}\right)\right)\end{aligned}$$

Now: if the chemotactic coefficient r is constant we get

$$\left\langle\frac{rS'}{v}\right\rangle = \frac{1}{\lambda}\frac{r}{v}\left\{S(z_0+\lambda)-S(z_0)\right\}=0$$

due to the periodicity of the traveling wave $\Rightarrow$ to leading order there is no chemotactic response on average: the amoeba is attracted as much to the front of the wave as it is repelled by the back.

At $\mathcal{O}\left(\frac{1}{v^2}\right)$ one gets

$$\bar{v} = v\left\langle\left(\frac{rS'}{v}-\left\langle\frac{rS'}{v}\right\rangle\right)^2\right\rangle \qquad \Rightarrow \qquad \text{sign}\bar{v}=\text{sign}v$$

The amoeba drifts in the same direction as the wave propagates: the amoeba is *advected*, i.e. it moves *away* from the source of the wave.

This is *independent* of the sign of the chemotactic coefficient r and of the wave profile of the chemoattractant: whenever the amoeba is moving towards the wave the time it is exposed to the gradient is shorter than when it moves with the wave $\Rightarrow$ the motion *with* the wave is enhanced compared to the motion against it.

How can the amoeba move towards the source of the wave? It needs to respond to the front of the wave differently than to the back.

Possibilities:

- the chemotactic coefficient r adapts to the concentration, i.e. it depends on the concentration with some delay (Nakajima et al., 2014)[16]
- the amoeba moves only briefly and becomes unresponsive once it has moved, like a refractory period for motion.

Kessler and Levine proposed and analyzed a minimal agent-based model for the chemotactic aggregation (Kessler and Levine, 1993).

[16]Their videos NakSaw14_s2,3.mov (on Canvas) show that the amoebae do not back up when they are under the back of the wave.